Am J Cancer Res 2022;12(1):396-426
www.ajcr.us /ISSN:2156-6976/ajcr0140710

Original Article

Novel insights linking BRCA1-IRIS role in mammary gland development to formation of aggressive PABCs: the case for longer breastfeeding

Patricia Castillo[1], Omonigho Aisagbonhi[2], Cheryl C Saenz[3], Wael M ElShamy[1]

[1]Breast Cancer Program, San Diego Biomedical Research Institute, [2]Department of Pathology, [3]Department of Obstetrics, Gynecology and Reproductive Sciences, UC San Diego Health System, San Diego, CA 92121, USA

Received November 22, 2021; Accepted December 27, 2021; Epub January 15, 2022; Published January 30, 2022

Abstract: Pregnancy-associated breast cancer (PABC) is diagnosed during or shortly after pregnancy. Although rare, PABC is a serious occurrence often of the triple negative (TNBC) subtype. Here we show progesterone, prolactin, and RANKL upregulate BRCA1-IRIS (IRIS) in separate and overlapping subpopulations of human mammary epithelial cell lines, which exacerbates the proliferation, survival, and the TNBC-like phenotype in them. Conversely, vitamin D_3 reduces IRIS expression in TNBC cell lines, which attenuates growth, survival, and the TNBC-like phenotype in them. In the mouse, Brca1-Iris (Iris, mouse IRIS homolog) is expressed at low-level in nulliparous mice, increases ~10-fold in pregnant/lactating mice, to completely disappear in involuting mice, and reappears at low-level in regressed glands. Mice underwent 3 constitutive pregnancies followed by a forced involution (after 5 days of lactation) contained ~10-fold higher Iris in their mammary glands compared to those underwent physiological involution (after 21 days of lactation). While protein extracts from lactating glands promote proliferation in $IRIS^{low}$ and IRIS overexpressing (IRISOE) cells, extracts from involuting glands promote apoptosis in $IRIS^{low}$, and aneuploidy in IRISOE cells. In a cohort of breast cancer patients, lack of breastfeeding was associated with formation of chemotherapy resistant, metastatic IRISOE breast cancers. We propose that terminal differentiation triggered by long-term breastfeeding reduces IRIS expression in mammary cells allowing their elimination by the inflammatory microenvironment during physiological involution. No/short-term breastfeeding retains in the mammary gland IRISOE cells that thrive in the inflammatory microenvironment during forced involution to become precursors for aggressive breast cancers shortly after pregnancy.

Keywords: Mammary gland, pregnancy' hormones, growth factors, and cytokines, BRCA1-IRIS, lactation, involution, TNBC, microenvironment, aneuploidy

Introduction

In humans and mice during pregnancy, progesterone (P_4), prolactin (PRL), interleukin (IL)-4, and receptor activator of NF-κB ligand (RANKL) cooperate to promote mammary gland growth, maturation, alveolar (secretory) cells formation [1], and increase vascularization in order to prepare the mammary gland for lactation [2-9] (Figure S1A-step-1). Exogenous P_4 stimulates pre-pubertal ovariectomized female mice mammary epithelial cell proliferation and terminal end bud formation in the absence of estrogen (E_2) [3]. P_4-bound progesterone receptor (PR) complex enters the nucleus to bind and activates transcription of a selected set of promoters that are directly involved in ductal elongation [3, 10-12].

Prolactin (PRL) level increases in the mammary gland during early pregnancy and along with P_4, triggers luminal progenitors' proliferation and differentiation into alveolar cells [2-9, 13] (Figure S1A-step-2). The prolactin receptor (PRLR) and PR colocalize in nulliparous female mice ductal epithelium [14]. Genetic studies suggest P_4 and PRL promote each other's expression and function [7, 10, 15, 16]. Paradoxically, high PRL levels were also observed in premenopausal women with a family history of breast cancer [17-19], and were associated with increased breast cancer risk

[20, 21]. PRL binding to PRLR on normal mammary epithelial and breast cancer cells activates STAT5 through Janus tyrosine kinase 2 (JAK2) [22, 23] to promote transcription of a plethora of proliferation and differentiation genes [24, 25]. Interestingly, constitutively activate, and nuclear STAT5 are found in >70% of invasive breast adenocarcinomas [26, 27].

In normal mammary glands, the osteoclast differentiation factor, RANKL [28] is secreted by mature PR^{+ve}-luminal "sensor" cells in response to P_4 and/or PRL. RANKL activates its receptor, RANK expressed on PR^{-ve}-luminal "responder" progenitors and basal cells [29, 30], suggesting a role for RANKL in the expansion of a specific subset of mammary luminal cells [31-37]. Since BRCA1 triggers luminal progenitor cells (LPCs) differentiation by enhancing FOXA1, GATA3, and ERα expression [38], it is believed that RANK signaling in LPCs amplifies the TNBC phenotype in BRCA1 mutation carriers [39]. Accordingly, RANK inactivation delays BRCA1 tumor onset, and offsets their progression to higher grades [34, 39].

The hormone, vitamin D_3 (VD_3) is associated with calcium and phosphate transport in the bones. VD_3 arrests growth of the mammary gland by upregulating the expression of differentiation factors and/or promoting apoptosis (Figure S1A-step-3) [40]. VDR, the receptor for VD_3 is localized predominantly to differentiated epithelial cells in the mouse, and its expression increases 100-fold during lactation [41]. VDR knockout mice show excess proliferation and side-branching and impaired apoptosis during involution (Figure S1A-step-3) [42-45]. Analysis of these mice showed that VD_3 signaling inhibits cyclin D1, p21, clusterin, β-catenin, and TGF-β1 expression in the mammary gland [42, 43]. In breast cancer cells, non-physiological concentrations of VD_3 are required to elicit growth arrest and apoptosis [46]. VD_3 signaling suppress cancer cell invasion, angiogenesis, and metastasis, by a so far unidentified mechanism [47].

The oncogene, BRCA1-IRIS (hereafter IRIS) is generated by the differential usage of the *BRCA1* locus [48]. In human, the expression levels of IRIS *mRNA* and protein increase significantly in breast cancer cell lines and tumors, especially those of the TNBC subtype [49-51]. Deliberate IRIS overexpression (IRISOE) in normal mammary epithelial cells promotes formation of cells exhibiting the TNBC phenotype (i.e., expressing stemness, epithelial-to-mesenchymal transition [EMT], and basal gene signatures), *in vitro* and TNBC tumors, *in vivo* [49, 50, 52]. Although the mouse IRIS, Brca1-Iris (Iris) shares only ~65% homology with IRIS [53], the two are functionally similar [54]. *IRIS* and *Iris mRNAs* and proteins consist of the first 11 exons of BRCA1 (Brca1) *plus* an in-frame reading extensions of 34 (human) [48] or 100 (mouse) [53] amino acids from intron 11 (*aka. I*n-frame *R*eading of BRCA1 *I*ntron 11 Splice variant). Moreover, IRIS- or Iris-silenced cells fail to generate tumors in immunocompromised or immunocompetent mice, respectively [52, 54].

The purpose of this study was to determine the effect of the pregnancy/lactation/involution microenvironments on the expression of IRIS/Iris in normal mammary epithelial cells and to find out whether the inflammatory microenvironment initiated in the mammary gland during forced involution (i.e., after no/short-term breastfeeding) is a promoter of, while the inflammatory microenvironment initiated during physiological involution (i.e., after long-term breastfeeding) is a protective against formation of IRIS/Iris-overexpressing PABCs shortly after pregnancy.

Materials and methods

Cell culture, hormone, cytokines, growth factors, and drugs

Commercially available cell lines are from ATCC maintained as per supplier instructions. The generation and maintenance of the doxycycline (Dox, 2 μg/ml, for 72 h)-inducible IRISOE cell lines (IRIS3, 5, 9, 10, 16, and 17) were described earlier [48]. Some of these cell lines were used to develop the orthotopic primary (1°) IRISOE-mammary tumors in athymic mice [50, 52]. From these tumors we developed the orthotopic 1° IRISOE mammary tumor cell lines, named IRIS291-IRIS295 [55]. All commercial and in-house cell lines were authenticated by STR profiling and tested for mycoplasma contamination.

Human recombinant P4 (P0130) and VD_3 (D1530) from Sigma, PRL (4687) from Bio-Vision, RANKL (ab9958) from abcam. 573108

(inhibitor I, inhibits SH2 domain), IQDMA (420294/inhibitor II), LY294002 (440202), and PP2 (P0042) from Calbiocam, and JSH-23 (J4455), and SP600125 (S5567) from Sigma.

Antibodies

Mouse anti-human IRIS and rabbit anti-mouse Iris were developed in our laboratory. Rabbit anti-human and mouse γ-Tubulin (ab11321, Abcam). Mouse anti-human PRLR (ab2772, abcam). Rabbit anti-human and mouse β-actin (4970, Cell Signaling). Rabbit anti-human H2B (ab18977, abcam). Mouse anti-human CK5 (MA5-17057, Thermo-Fisher). Rabbit anti-human CK17 (ab51056, abcam). Rabbit anti-human EGFR (ab52894, abcam). Mouse anti-human CDH2 (610920, BD Bioscience). Mouse anti-human TWIST (ab50887, abcam). Rabbit anti-human SLUG (C19G7, Cell signaling). Mouse anti-human Oct4 (sc-5279, Santa Cruz). Mouse anti-human and mouse Sox2 (L1D6A2, Cell Signaling). Goat anti-human Nanog (AF1997, R&D). Rabbit anti-human VDR (D2K6W, Cell Signaling). Mouse anti-human RANK (NB100-56508, Novousbio). Goat anti-human NF-κB/p65 (sc-372, Santa Cruz). Mouse anti-human STAT3 (MAB1799, R&D). Rabbit anti-human p-STAT3^{Y705} (9145, Cell Signaling). Rabbit anti-human STAT5 (sc-835, Sant Cruz). Rabbit anti-human p-STAT5^{Y694} (C11C5, Cell signaling). Rabbit anti-human Cyclin D1 (RB-010-P0, Thermo-Scientific). To detect BRCA1/p220 we used the mouse monoclonal antibody SG-11 (Calbiochem, San Diego, Calif), while anti-pCBP$_2$ was from Sigma.

Proliferation and apoptosis assays

Performed using the Promega MTS kit (G3582), and Caspase-Glo 3/7 Kit (G8090) following the manufacturer's instructions. Assays done 3 separate times, each at least in triplicates.

siRNA transfection and generation of shIRIS cells lines

Naïve HME, MDA-MB231 (aka 231), MDA-MB-453 (453), MDA-MB-468 (468), or BT-594 cells were seeded at low density. Transient transfection of siRNAs (siLuc, siIRIS, siPRLR, or siVDR) was carried out using Xfect™ Transfection reagent (Clonetech Laboratories, Inc., Mountain View, CA, USA) according to the manufacturer's instructions. After 48 h, the media were changed, and cells were incubated to different time points after that. Generation of the 231, 468, and 453 cell lines expressing shCtrl or shIRIS, as well as 4T1 or EO771 expressing shCtrl or shIris was described previously [50, 55].

Quantitative real-time RT/PCR

Performed as previously described [56] using total RNA isolated by TRIzol reagent (Invitrogen, Carlsbad, CA, USA) according to the manufacturer's protocol. Briefly, 100 ng of total RNA was analyzed by qRT/PCR using iScript™ One-Step RT-PCR kit with SYBR Green (Bio-Rad, Hercules, CA, USA), according to the manufacturer's instructions. Expression was normalized to *GAPDH/Gapdh* expressed in the same sample. Assays were done in triplicates 3 separate times. Primer sequences are listed below:

*Human genes (related to **Figures 1E, 1G, 2C-E, 3B, 4B, 4D, 4I, 5B** and **5F**):* IRIS Forward primer: 5'-GTCTGAGTGACAAGGAATTGGTTT-3'; IRIS Reverse primer: 5'-TTAACTATACTTGGAAATTTGTAAAATGTG-3'; GAPDH Forward primer: 5'-AATGGAAATCCCATCACCATCT-3'; GAPDH Reverse primer: 5'-CGCCCCACTTGATTTTGG-3'.

*Basal activators (related to **Figures 3C, 4I,** and **5F**):* CK5 Forward primer: 5'-GCGGTTCCTGGAGCAGCAGAACAAGGTTCT-3'; CK5 Reverse primer: 5'-CTGAGGTGTCAGAGACATGCGTCTGCATCT-3'; CK17 Forward primer: 5'-CTGGCTGCTGATGACTTCCGCACCAAGTTT-3'; CK17 Reverse primer: 5'-CGCAGTAGCGGTTCTCTGTCTCCGCCAGGT-3'; EGFR Forward primer: 5'-CCAGGACCCCCACAGCACTGCAGTGGGCAA-3'; EGFR Reverse primer: 5'-GTGGGTGTAAGAGCTAATGCGGGCATGGCA-3'.

*EMT promoters (related to **Figures 3E, 4I,** and **5F**):* CDH2 Forward primer: 5'-ACAGTGGCCACCTACAAAGG-3'; CDH2 Reverse primer: 5'-CCGAGATGGGGTTGATAATG-3'; Twist Forward primer: 5'-GGAGTCCGCAGTCTTACGAG-3'; Twist Reverse primer: 5'-TCTGGAGGACCTGGTAGAGG-3'; SLUG Forward primer: 5'-GGGGAGAAGCCTTTTTCTTG-3'; SLUG Reverse primer: 5'-TCCTCATGTTTGTGCAGGAG-3'.

*Stemness inducers (related to **Figures 3D, 4I, and 5F**):* Oct4 Forward primer: 5'-ACATGTGTAAGCTGCGGCC-3'; Oct4 Reverse primer:

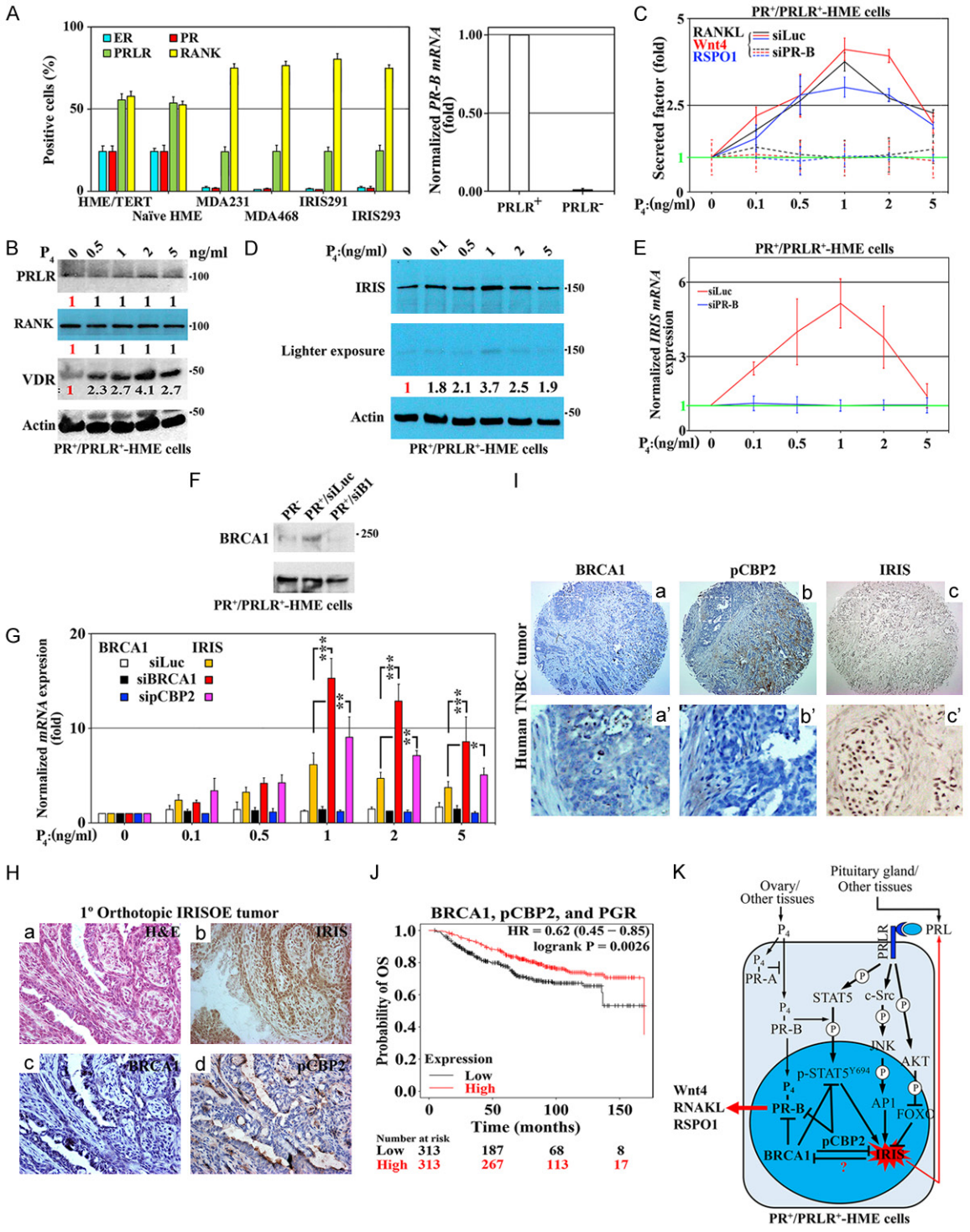

Figure 1. P_4 effect on IRIS expression in PR^{+ve}-HME cells. (A) Percentage of ER^{+ve}, PR^{+ve}, $PRLR^{+ve}$, and $RANK^{+ve}$ populations within HME cell lines as defined by FACS analysis (left). Normalized PR-B expression within the $PRLR^{-ve}$- or $PRLR^{+ve}$-HME cells (right). (B) PRLR, RANK, and VDR expression in $PR^{+ve}/PRLR^{+ve}$-HME cells treated with increasing concentration of P_4 for 24 h. (C) RANKL, Wnt4, and RSPO1 secretion from $PR^{+ve}/PRLR^{+ve}$-HME cells treated with increasing concentration of P_4 for 24 h. (D) IRIS protein expression in $PR^{+ve}/PRLR^{+ve}$-HME cells treated with increasing concentration of P_4 for 24 h. (E) *IRIS mRNA* expression in $PR^{+ve}/PRLR^{+ve}$-HME cells transfected with siLuc or siPR-B for 48 h and treated with increasing concentration of P_4 for an additional 24 h. (F) BRCA1 expression in PR^{-ve} or PR^{+ve}-HME cells transfected with siLuc or siBRCA1 for 48 h then with increasing concentration of P_4 for an additional 24 h. (G) *BRCA1 or IRIS mRNAs* expression in $PR^{+ve}/PRLR^{+ve}$-HME cells transfected with siLuc, siBRCA1, ore sipCBP2

for 48 h then treated with increasing concentration of P_4 for an additional 24 h. (H) IHC analysis of H&E (a), IRIS (b), BRCA1 (c), and $pCBP_2$ (d) on 1°-orthotopic IRISOE tumor developed in athymic mice. (I) IHC analysis of BRCA1 (a, a'), $pCBP_2$ (b, b'), and IRIS (c, c') on human TNBC tumor. (J) TCGA analysis of the probability of OS for BRCA1, $pCBP_2$, and PGR high (red) vs. low (black) expressors breast cancer patients. In all parts n=3. (K) Model representing the data presented above.

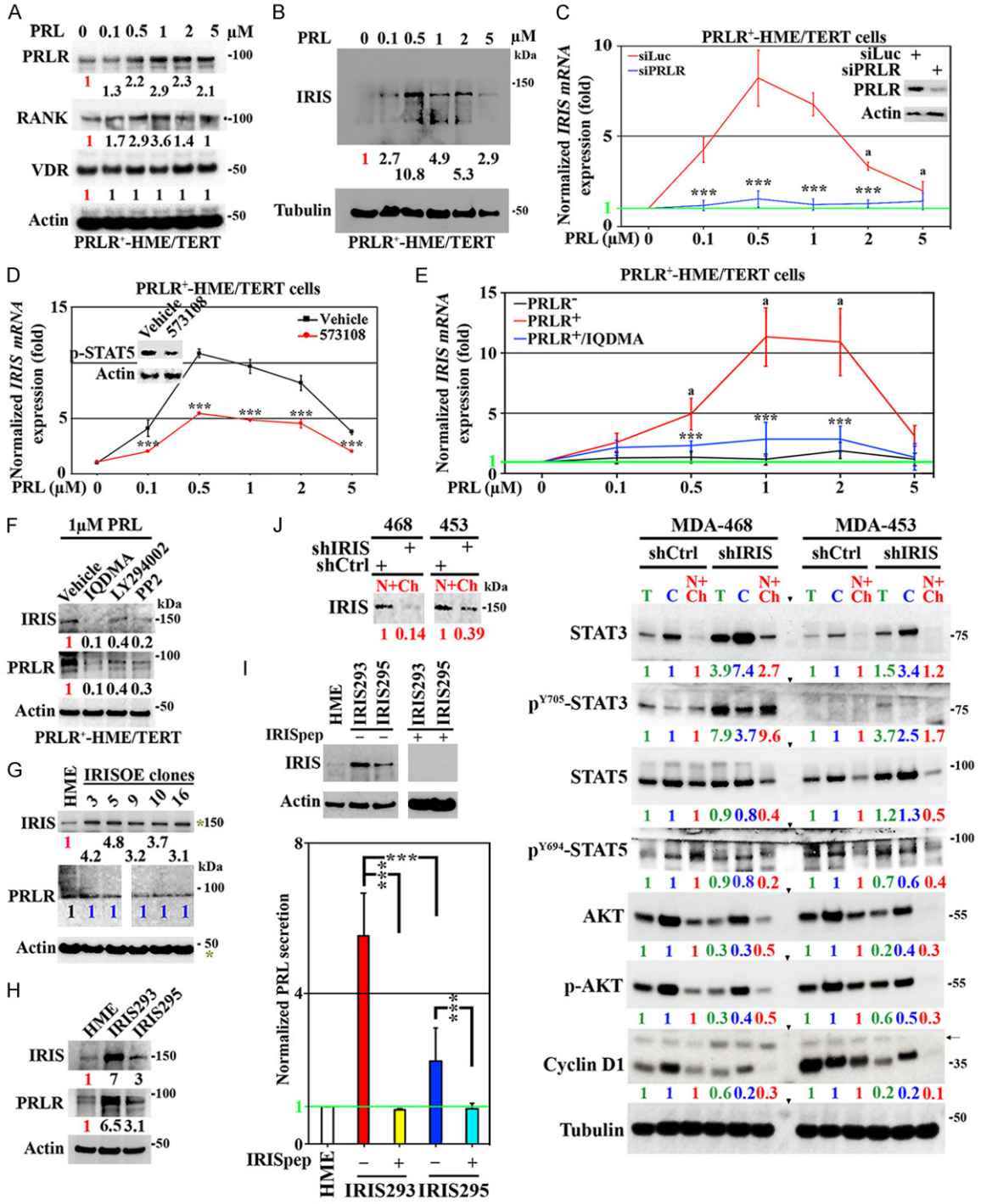

Figure 2. PRL effect on IRIS expression in $PRLR^{+ve}$-HME cells. A. PRLR, RANK, and VDR expression in $PRLR^{+ve}$-HME cells treated with increasing concentration of PRL for 24 h. B. IRIS protein expression in $PRLR^{+ve}$-HME cells treated with increasing concentration of PRL for 24 h. C. Normalized *IRIS mRNA* expression in $PRLR^{+ve}$-HME cells transfected with siLuc or siPRLR for 48 h (inset) and treated with increasing concentration of PRL for an additional 24 h. D.

Normalized *IRIS mRNA* expression in $PRLR^{+ve}$-HME cells treated with vehicle or 573108 (inset) and increasing concentration of PRL for 24 h. E. Normalized *IRIS mRNA* expression in $RPLR^{-ve}$ or $PRLR^{+ve}$-HME cells treated with vehicle or IQDMA and increasing concentration of PRL for 24 h. F. IRIS and PRLR expression in $PRLR^{+ve}$-HME cells treated with 1 μM PRL in the presence of vehicle, IQMDA, LY294002, or PP2 for 24 h. G. IRIS and PRLR expression in parental HME or several Dox-inducible HME/IRIS cell clones (induced 72 h). H. IRIS and PRLR expression in parental HME, IRIS293 or IRIS295 cell lines. I. Expression of IRIS protein (top) or PRL secretion (bottom) from parental HME, IRIS293 or IRIS295 treated with scrambled (-) or IRISpep for 24 h. J. Expression of IRIS (inset), and the levels of total then stripped and blotted for Y^{705}-phosphorylated STAT3, total then stripped and blotted for Y^{694}-phosphorylated STAT5, total then stripped and blotted for $T^{308}S^{473}$-phosphorylated AKT and Cyclin D1 in total (T), cytoplasmic (C), and nuclear+chromatin (N+Ch) extracts from MDA-MB468 and MDA-MB-453 cell lines expressing shCtrl or shIRIS. Arrow indicate non-specific band. In all parts n=3.

5'-GTTGTGCATAGTCGCTGCTTG-3'; Sox2 Forward primer: 5'-TTCATCGACGAGGCTAAGCGGCTG-3'; Sox2 Reverse primer: 5'-AGCTGCCGTTGCTCCAGCCGTTCA-3'; Nanog Forward primer: 5'-ATGCCTCACACGGAGACTGT-3'; Nanog Reverse primer: 5'-AGGGCTGTCCTGAATAAGCA-3'.

*Decreased in IRISOE cells (related to **Figure 6H**):* JAK1 Forward primer: 5'-GAGACAGGTCTCCCACAAACAC-3'; JAK1 Reverse primer: 5'-GTGGTAAGGACATCGCTTTTCCG-3'; MOBA1 Forward primer: 5'-TGTTGCCTGAGGGAGAGGATCT-3'; MOBA1 Reverse primer: 5'-GCAGACATGACTGGACAGCTTG-3'; MFN1 Forward primer: 5'-GGTGAATGAGCGGCTTTCCAAG-3'; MFN1 Reverse primer: 5'-TCCTCCACCAAGAAATGCAGGC-3'; STAP1 Forward primer: 5'-GGAGGATTGAGACAGAGCAGAG-3'; STAP1 Reverse primer: 5'-CTTCTGGAGCATCTCAGTTGCC-3'; SPZ1 Forward primer: 5'-GGAACAGGTGAAGAAACTGAGCC-3'; SPZ1 Reverse primer: 5'-GCTTCTCTTGCAGAGTTCCCTG-3'; TESTIN Forward primer: 5'-GTGGCAGACATTACTGTGACAGC-3'; TESTIN Reverse primer: 5'-CAGCAGAAGTGTTTCAGGTGCC-3'; PPP3R2 Forward primer: 5'-GGAGCAGAAGTTGAGGTTTGCG-3'; PPP3R2 Reverse primer: 5'-CCACCATCATCTTCAGCACCTG-3'; KCDT14 Forward primer: 5'-GTACCGTGAGGCTCAGTTCTACGAAATC-3'; KCDT14 Reverse primer: 5'-CCAGGGCCCAAACTTACAACAGACTTGAAC-3'; GNG2 Forward primer: 5'-ATGGAAGCCAATATCGACAGGATA-3'; GNG2 Reverse primer: 5'-CTTCTCCCTAAACGGGTTTTCTG-3'; CDYL2 Forward primer: 5'-CGCCAGAATGAAAGCAACTGTCG-3'; CDYL2 Reverse primer: 5'-GTCGTCTGTGGCTGCGTTGCA-3'; FGS4 Forward primer: 5'-CAGGAATCCTCCAAGCGATGCA-3'; FGS4 Reverse primer: 5'-CTTCATGTGCCACTACGTCGTG-3'.

*Increased in IRISOE cells (related to **Figure 6I**):* ST6GAL2 Forward primer: 5'-CAACCAAACCCACCATCTTCTGG-3'; ST6GAL2 Reverse primer: 5'-AGTACAGCTCGTGGTAGTGGCA-3'; LPP Forward primer: 5'-GCCGGCACTGAGAAGAACGAACACAAG-3'; LPP Reverse primer: 5'-CCACACTAAGAAAAGCCATTCAACCAGAT-3'; FGFR1 Forward primer: 5'-GCACATCCAGTGGCTAAAGCAC-3'; FGFR1 Reverse primer: 5'-AGCACCTCCATCTCTTTGTCGG-3'; TLE1 Forward primer: 5'-AGGATGCTTCTAGCAGTCCAGC-3'; TLE1 Reverse primer: 5'-GTGTGCTGGATTTCAGAACAGGC-3'; KCNMA1 Forward primer: 5'-TATCTCTCCAGTGCCTTCGTGG-3'; KCNMA1 Reverse primer: 5'-CTCTCTCGGTTGGCAGACTTGT-3'; LGR4 Forward primer: 5'-GGAGCATTTGATGGTAATCCACTC-3'; LGR4 Reverse primer: 5'-CCATGCTTGCACCACGAATGAC-3'; ARF6 Forward primer: 5'-CCAAGGTCTCATCTTCGTAGTGG-3'; ARF6 Reverse primer: 5'-AGGTCCTGCTTGTTGGCGAAGA-3'; CX3CL1 Forward primer: 5'-ACAGCACCACGGTGTGACGAAA-3'; CX3CL1 Reverse primer: 5'-AACAGCCTGTGCTGTCTCGTCT-3'; SUZ12 Forward primer: 5'-CCATGCAGGAAATGGAAGAATGTC-3'; SUZ12 Reverse primer: 5'-CTGTCCAACGAAGAGTGAACTGC-3'; NDC80 Forward primer: 5'-CTGACACAAAGTTTGAAGAAGAGG-3'; NDC80 Reverse primer: 5'-TAAGGCTGCCACAATGTGAGGC-3'; PAK5 Forward primer: 5'-TGAGGAGCAGATTGCCACTGTG-3'; PAK5 Reverse primer: 5'-CTGAGCACAGAATCCGAAGTCC-3'.

*Mouse genes (related to **Figure 6D, 6E, 6J** and **6K**):* Iris Forward primer: 5'-GTGGGAATGAGGAAGCTTTCC-3'; Iris Reverse primer: 5'-CCACCCGAAATCTCTCTAGCC-3'; GAPDH Forward primer: 5'-AACTTTGGCATTGTGGAAGG-3'; GAPDH Reverse primer: 5'-ACACATTGGGGGTAGGAACA-3'.

*Involution inhibitors (related to **Figure 6L**):* IRF-1 Forward primer: 5'-TCCAAGTCCAGCCGAGACACTA-3'; IRF-1 Reverse primer: 5'-ACTGCTGTGGTCATCAGGTAGG-3'; SREBF-1 Forward primer: 5'-TGTTGGAGGACTCGCTTCTGCA-3'; SREBF-1 Reverse primer: 5'-CCACACCTCAATGTCGTCCATG-3'; Sim2s Forward primer: 5'-CGGAGATCAAGCTCCACAGCAA-3'; Sim2s Reverse prim-

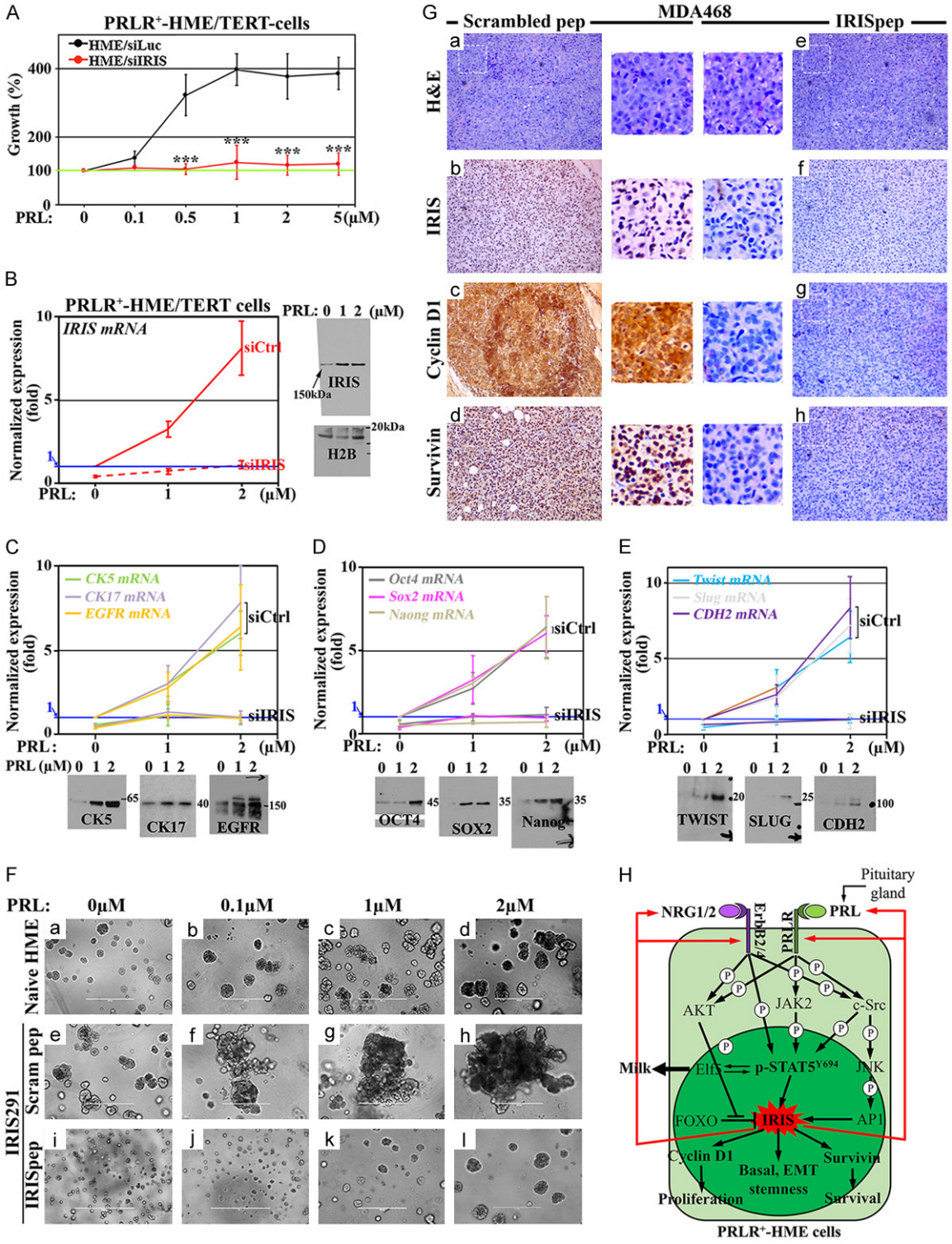

Figure 3. PRL-induced IRIS triggers proliferation, survival, the TNBC phenotype in PRLR^{+ve}-HME cells. (A) Percentage growth in PRLR^{+ve}-HME cells transfected with siLuc or siIRIS for 48 h and treated with increasing concentration of PRL for an additional 24 h. (B) Normalized *IRIS mRNA* expression (left) and protein (right) in PRLR^{+ve}-HME cells transfected with siLuc or siIRIS for 48 h and treated with increasing concentration of PRL for an additional 24 h. (C) Normalized *CK5, CK17, and EGFR mRNAs* (top) and proteins expression (bottom) in PRLR^{+ve}-HME cells transfected with siLuc or siIRIS for 48 h and treated with increasing concentration of PRL for an additional 24 h. (D) Normalized *Oct4, Sox2, and Nanog mRNAs* (top) and proteins expression (bottom) in PRLR^{+ve}-HME cells transfected with siLuc

or siIRIS for 48 h and treated with increasing concentration of PRL for an additional 24 h. (E) Normalized *Twist, Slug, and CDH2 mRNAs* (top) and proteins expression (bottom) in PRLR^{+ve}-HME cells transfected with siLuc or siIRIS for 48 h and treated with increasing concentration of PRL for an additional 24 h. (F) MSF assay using naïve HME cells, or IRIS291 treated with scrambled or IRISpep *plus* increasing concentrations of PRL for 24 h. (G) IHC analysis of H&E (a and e), IRIS (b and f), Cyclin D1 (c and g), and survivin (d and h) on orthotopic MDA-MB-468 tumors treated with scrambled or IRISpep. In all parts n=3. (H) Schematic representation of the data in **Figures 2** and **3**.

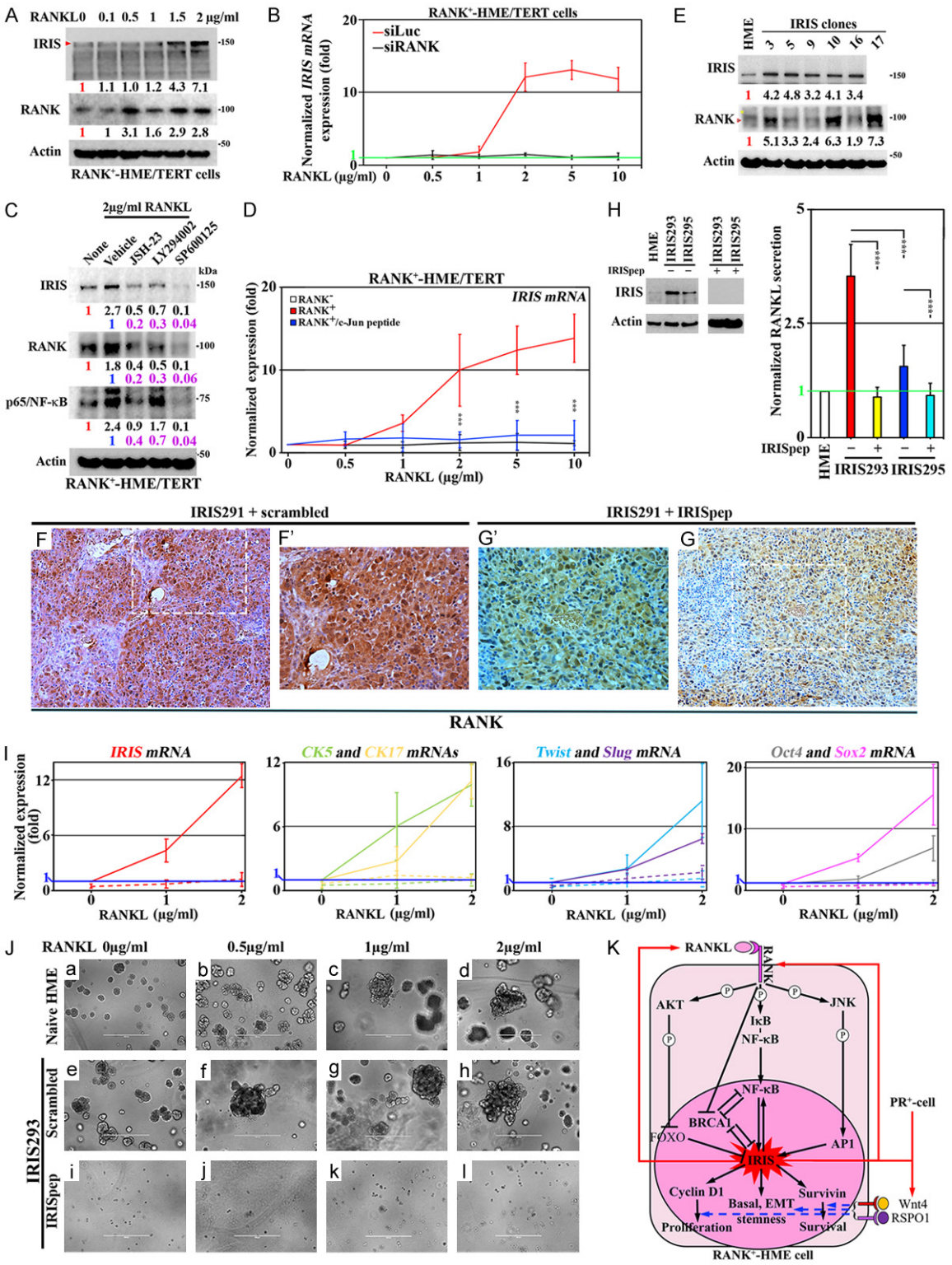

Figure 4. Positive feedforward loop between IRIS and RANKL/RANK signaling in RANK^{+ve}-HME cells. (A) IRIS and RANK expression in RANK^{+ve}-HME cells treated with increasing concentrations of RANKL for 24 h. (B) Normalized *IRIS mRNA* expression in RANK^{+ve}-HME cells transfected with siLuc or siRANK for 48 h and treated with increasing concentration of PRL for an additional 24 h. (C) IRIS, RANK, and NF-κB/p65 expression in RANK^{+ve}-HME cells treated with 2 μg/ml of RANKL in the presence of none, vehicle, JSH-23, LY294002 or SP600125 for 24 h. (D) Normalized *IRIS mRNA* expression in RANK^{-ve} or RANK^{+ve}-HME cells transduced with scrambled or c-Jun inhibitory peptide and treated with increasing concentrations of RANKL for 24 h. (E) Expression of IRIS and RANK in parental HME or several inducible HME/IRIS cell lines treated with Dox for 72 h. Some blots are used in **Figure 2G**. (F-G') Expression of RANK on IRIS291 tumor treated with scrambled (F, F') or IRISpep (G, G'). (H) Expression of IRIS protein (top) or RANKL secretion (bottom) from parental HME, IRIS293 or IRIS295 treated with scrambled (-) or IRISpep for 24 h. Some blots are used in **Figure 2I**. (I) Normalized *IRIS* (left), *CK5* and *CK17* (middle left), *Twist, Slug* (middle right), and *Oct4, Sox2* (right) expression in RANK^{+ve}-HME cells transfected with siLuc or siIRIS for 48 h and treated with increasing concentration of RANKL for an additional 24 h. (J) MSF assay using naïve HME cells, or IRIS293 cells treated with scrambled or IRISpep *plus* increasing concentrations of RANKL for 24 h. In all parts n=3. (K) Schematic representation of the data above.

er: 5'-CGATCAGGTCTTGTGGCTCATAG-3'; ADIPOQ Forward primer: 5'-AGATGGCACTCCTGGAGAGAAG-3'; ADIPOQ Reverse primer: 5'-ACATAAGCGGCTTCTCCAGGCT-3'; IGF-1 Forward primer: 5'-CGGGATCTCATCAGCTTCACAG-3'; IGF-1 Reverse primer: 5'-TCCTTGTTCGGAGGCAGGTCTA-3'; JAK2 Forward primer: 5'-GCTACCAGATGGAAACTGTGCG-3'; JAK2 Reverse primer: 5'-GCCTCTGTAATGTTGGTGAGATC-3'.

*Involution activators (related to **Figure 6L**):* IGFBP5 Forward primer: 5'-AAGAGCTACGGCGAGCAAACCA-3'; IGFBP5 Reverse primer: 5'-GCTCGGAAATGCGAGTGTGCTT-3'; cEBP Forward primer: 5'-TCCACGACTCCTGCCATGTACG-3'; cEBP Reverse primer: 5'-GTGGTTGCTGTTGAAGAGGTCG-3'; LIF Forward primer: 5'-CTTCGATCCTCAACACAGAGCAG-3'; LIF Reverse primer: 5'-CGCTTGCTCTACTGTGATGTCG-3'; FasL Forward primer: 5'-GAAGGAACTGGCAGAACTCCGT-3'; FasL Reverse primer: 5'-GCCACACTCCTCGGCTCTTTTT-3'; ATF4 Forward primer: 5'-AACCTCATGGGTTCTCCAGCGA-3'; ATF4 Reverse primer: 5'-CTCCAACATCCAATCTGTCCCG-3'; CathapsinL Forward primer: 5'-GGGGCATGGGTGGCTACGTAAAGAT-3'; CathapsinL Reverse primer: 5'-GCGGGGGCTGGTAGACTGAAGATGAA-3'.

Western blot

Performed, as previously described [56]. Briefly, protein lysates were prepared from membrane fraction or whole cell extracts by sonication in PBS containing protease and phosphatase inhibitor tablets (Thermo Scientific, Waltham, MA, USA) according to the manufacturer's instructions. Protein concentration was estimated using the Pierce™ BCA protein assay kit (Thermo Scientific, Waltham, MA, USA). Cell lysates were denatured in NuPAGE LDS sample buffer (Thermo Scientific) and were resolved on NuPAGE gels (Thermo Scientific) and electrotransferred to PVDF membrane. The membrane was blocked with 5% dry milk for 1 h, washed thrice with PBST, and subsequently incubated with primary antibody overnight at 4°C. The next day, blots were washed thrice with PBST and incubated with HRP-conjugated secondary antibody for 1 h at RT, washed and developed using Western Lightning Plus-ECL as a substrate. Tubulin and actin were used as an internal loading control. Each blot was repeated 2-3 times.

Immunohistochemistry

All animal experiments were approved by the "Institutional Animal Care and Use Committee" (IACUC) of the University of Mississippi Medical Center and in accordance with the NIH guidelines. Immunohistochemical analysis was performed as previously described [56] on 4 μm thick paraffin-embedded sections of tumor tissue excised from IRIS291-IRIS295 orthotopic mammary tumor generated in Nu/Nu mice. Briefly, sections deparaffinized, rehydrated, and washed in PBS were processed for antigen retrieval for IRIS staining by incubating in pepsin (10 μM) for 20 min at 37°C. All other antigen retrievals were by boiling slides in citrate buffer (pH 6.0) for 10 min in a microwave. Slides cooled to RT, washed 3× PBS for 15 min each were incubated in 3% hydrogen peroxide (H_2O_2) for 10 min to block endogenous peroxidase activity. After washing, slides were blocked with 10% normal goat serum for 1 h at RT, washed and incubated with primary antibodies overnight at 4°C in a moist chamber. After 3× PBS washes, slides were

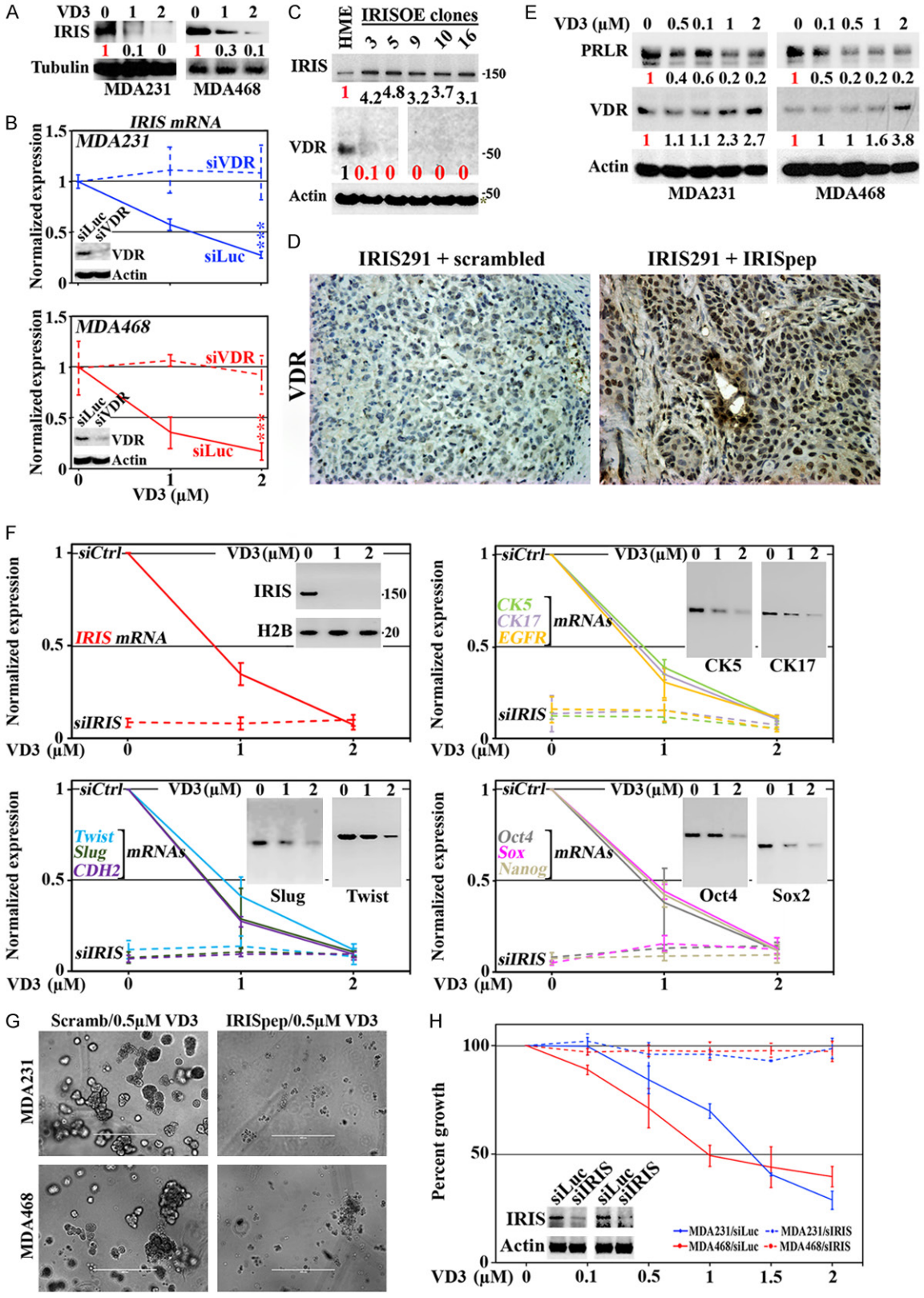

Figure 5. Negative feedback loop between IRISOE and VD_3/VDR activity in IRISOE-TNBC cells. A. Expression of IRIS in MDA231 and MDA468 cells 24 h after treatment with the indicated VD_3 concentrations. Data presented are representative of 3 separate times. B. Normalized *IRIS mRNA* expression in MDA231 (upper), MDA468 (lower) cells pre-silenced from control or VDR for 48 h followed by treatment with the indicated concentration of VD_3 for an additional

24 h. Data presented are from triplicates done three separate times. Inset shows the expression of VDR in these cells at 48 h after transfection. C. IRIS and VDR expression in parental HME and several inducible HME/IRIS cell lines treated with Dox for 72 h. Some blots are used in **Figure 2G**. D. IHC analysis of VDR on IRIS291 tumor treated with scrambled or IRISpep. E. Expression of PRLR and VDR in MDA231 or MDA468 cell lines treated with increasing concentrations of VD_3 for 24 h. F. Normalized *IRIS* (upper left), *CK5*, *CK17*, and *EGFR* (upper right), *Twist, Slug*, and CDH2 (lower left), and *Oct4, Sox2*, and Nanog (lower right) mRNA and proteins expression (insets) in MDA468 cells transfected with siLuc or siIRIS for 48 h and treated with increasing concentration of VD_3 for an additional 24 h. G. MSF assay using MDA231 and MDA468 cells treated with scrambled or IRISpep *plus* 0.5 μM of VD_3 for 24 h. H. Percentage of growth of MDA231 and MDA468 cells transfected with siLuc or siIRIS for 48 h (inset) then in SF-media with increasing concentrations of VD_3. In all parts n=3.

incubated with horseradish peroxidase (HRP) secondary antibody for 1 h at RT and washed with PBS. HRP-conjugated secondary antibody was developed with Vector DAB substrate kit (Vector Laboratories, Burlingame, CA, USA) and counterstained with Meyer's hematoxylin (Thermo Scientific) for 2 min, washed, dehydrated, and mounted with Permount (Thermo Fisher Scientific), and were imaged under the microscope.

TCGA meta-analysis using Kaplan Meier plotter

Meta-analysis-based biomarker assessment using the online tool Kaplan Meier Plotter (http://kmplot.com/analysis) to delineate the association between gene expression of genes separately or combined. Within each cohort, high expresser and low expresser patients were analyzed and compared for their overall survival (OS), distant metastasis-free survival (DMFS), or recurrent free survival (RFS). Normalized expression levels of genes analyzed were available for every patient in each cohort; the individual expression levels were summed, and each cohort was then dichotomized into patients with high or low expressions using the median of the summed expression levels in each cohort as the split-point. Subsequently, Kaplan-Meier plots and log-rank statistics were calculated to compare the subgroups with high or low expression.

Additionally, unidentified data from a cohort of recently diagnosed patients with locally advanced breast cancers (n=49) and treated at the National Cancer Institute (NCI), Cairo University (Cairo, Egypt) between September 2009 and October 2012 [57, 58] was personally communicated to us by Dr. Abeer Bahnessy (NCI, Egypt). Normal breast tissue samples (n=20) from females undergoing reduction mammoplasty (matched for age) were also used. Written informed consent was obtained from all participants before enrollment in the study. The Institutional Review Board (IRB) of the NCI, Cairo, Egypt, approved the protocol in accordance with the 2011 Declaration of Helsinki. Patients enrolled in the study were ≥18 years old, had an Eastern Cooperative Oncology Group (ECOG) Adequate performance: ≤2 [59], and exhibited adequate hematological parameters (WBC count, $\geq 3.0\times10^9$/l; ANC, $\geq 1.5\times10^9$/l; platelet count, $\geq 100\times10^9$/l; hemoglobin level, ≥9 g/l), liver function (serum bilirubin, <1.5×ULN; ALT and AST levels, <3 times normal values), and kidney function (plasma creatinine level, <1.5 times normal value) function. None of the patients were pregnant or breast-feeding, had an active second malignancy, or were involved in another clinical trial. The median follow-up period was 33 months.

Statistical analysis

Statistical analysis was performed using unpaired, two-tailed Student's t-test. In the case of comparing several data sets, One-way ANOVA test with Bonferroni post-hoc test was also conducted. In all figures, data represents the mean from at least 3 separate biological repeats done in at least in triplicates each +/- SD, $^{*}P<0.05$, $^{**}P<0.01$, and $^{***}P<0.001$.

Results

To rule out effects due to immortalization or expression of human TERT, many of the assays were also performed in naïve HME cells (i.e., non-immortalized and never cultured prior to use) with identical results. For simplicity, results using HME/TERT (hereafter HME) cells are presented. According to FACS analysis, HME cell lines encompass ~25% PR^{+ve} ($ER\alpha^{+ve}$), ~50% $PRLR^{+ve}$, and ~50% $RANK^{+ve}$ (**Figure 1A**-left), whereas endogenously IRISOE-TNBC cell lines (e.g., MDA231 [231], and MDA468

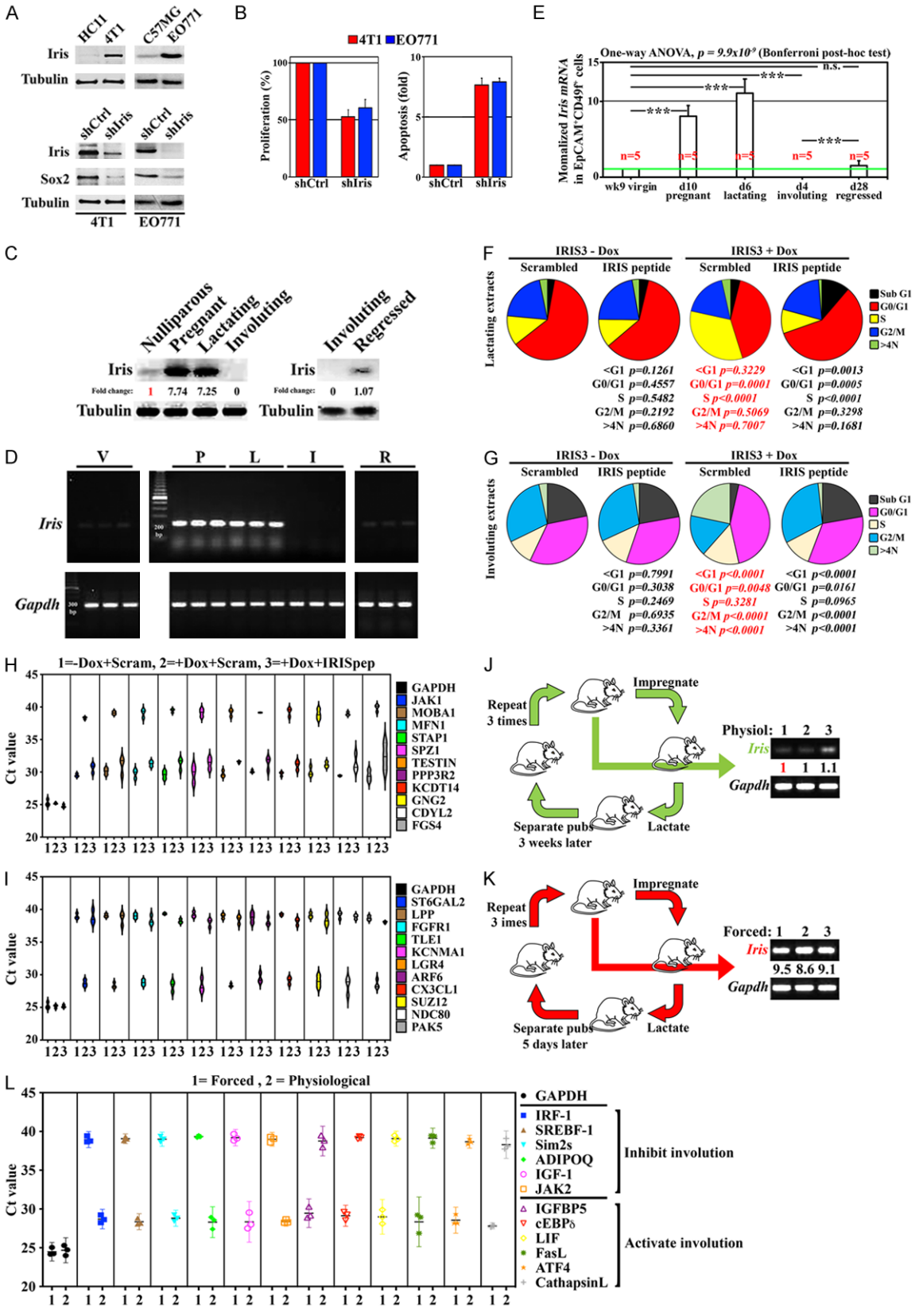

Figure 6. Iris expression during adult female mouse mammary gland development. (A) Comparison between the expression of Iris in HC11 or 4T1 (upper left), and C57MG or EO771 (upper right). The expression of Iris and Sox2 in 4T1 (lower left) or EO771 (lower right) cells expressing siCtrl or shIris. (B) Percentage BrdU incorporation (left) or

cleaved caspase 3/7 (right) in 4T1 (red) or E0771 (blue) cells expressing shCtrl or shIris. (C) Expression of Iris in nulliparous week (wk) 10, pregnant (P) day 15, lactating (L) d3, involuting (I) d3, and regressed (R) d28 C57BL/6 mice mammary glands. (D) Expression of *Iris mRNA* in nulliparous 10 (n=3), P-d15 (n=3), L-d3 (n=3), I-d3 (n=3), and R-d28 (n=3) C57BL/6 mice mammary glands. (E) Normalized *Iris* m*RNA* expression in EpCAM^{+}-cells FACS-sorted from nulliparous wk9 (n=5), P-d10 (n=5), L-d6 (n=5), I-d4 (n=5), and R-d28 (n=5) from BALB/c mice mammary glands. (F and G) Venn diagrams showing the cell cycle profile including sub-G1 (apoptotic), and >4N (tetraploid) in uninduced IRIS3 (-Dox) or induced IRIS3 (+Dox) cells treated with 500 µg of protein extracts from L-d10 (F) or I-d3 (G) BALB/c mice mammary glands (n=3ea, combined) in the presence of scrambled or IRISpep. Assays were repeated 3 separate times. (H and I) Ct values from RTqPCR analysis of the indicated *mRNAs* in similar cultures as in (G) treated as indicated, except the culture extended for additional 2 days before *RNAs* were prepared. Assays were repeated 3 separate times. (J and K) BALB/c mice (n=3/ea) were impregnated 3-consecutive times with full-term lactation (i.e., precedes physiological involution, J) or abrupt lactation at 5 days (i.e., precedes forced involution, K). Right sides show the level of *Iris mRNA* in the glands of these mice at the end of the experiments. (L) Ct values from RTqPCR analysis of the indicated *mRNAs* in the mammary glands from mice in (J and K). Assays were repeated 3 separate times.

[468]), or ectopically IRISOE (e.g., IRIS291 and IRIS293, for details see [52, 55]) encompass no PR^{+ve} (or ERα^{+ve}), ~25% PRLR^{+ve}, and ~75% are RANK^{+ve} (**Figure 1A**-left). All subsequent analysis performed on live cells obtained by FACS sorting of unfixed and unpermeabilized cells.

P_4-signaling triggers IRIS expression in PR^{+ve}-HME cells

RTqPCR showed that *PRG mRNA* is exclusively expressed in PRLR^{+ve}-HME cells (**Figure 1A**-right). To isolate PR^{+ve} cells we sorted PRLR^{+ve} (hereafter PR^{+ve})-HME cells and incubated them with 0-5 ng/ml of P_4 in growth-factors free (GFF)-medium for 24 h. P_4 treatment did not affect PRLR-long form (LF) or RANK expression (**Figure 1B**). However, as shown earlier [60-62], P4 treatment stimulated VDR expression (**Figure 1B**), and Wnt4, RANKL, and RSPO1 secretion (**Figure 1C**) from PR^{+ve}-HME cells in a biphasic manner peaking at 1-2 ng/ml. Additionally, P_4 treatment upregulated IRIS protein (**Figure 1D**), and *mRNA* (**Figure 1E**) expression also in a bi-phasic manner peaking at 1 ng/ml. Silencing PR-B not PR-A blocked the secretion of RANKL, Wnt4, and RSPO1, and the upregulation of IRIS (**Figure 1C**, **1E**, and data not shown), suggesting P_4/PR-B signaling directly or indirectly activates IRIS transcription.

BRCA1 inhibits P_4-induced IRIS expression in PR^{+ve}-HME cells by upregulating $pCBP_2$

$pCBP_2$ binds the 3'-UTR of certain *mRNAs* (e.g., oncogenes) and degrades them [63-65]. In HME cells, $pCBP_2$ expression is regulated by BRCA1 [63], and BRCA1 is expressed specifically in PR^{+ve}-HME cells (**Figure 1F**). Because $pCBP_2$ binds and degrades *IRIS mRNA* in HME cells [63], we proposed loss of BRCA1 expression (or function) as a potential mechanism to unleash IRISOE in TNBC cells. To study this here, we transfected PR^{+ve}-HME cells with luciferase (siLuc, control), BRCA1, or $pCBP_2$ siRNAs for 48 h (cf. **Figure 1F**, and data not shown). Equal numbers of silenced cells were then exposed in GFF-media to 0-5 ng/ml P_4 for another 24 h. P_4 upregulated *IRIS mRNA* expression to higher levels in siBRCA1- or sipCBP_2- compared to siLuc-transfected PR^{+ve} cells, also in biphasic manner peaking at 1 ng/ml (**Figure 1G**). Interestingly, The effect in siBRCA1-transfected cells was higher than that in sipCBP_2-transfected cells, perhaps due to BRCA1 induces expression of other *IRIS mRNA* degrading proteins, e.g., AUF1 [63], suggesting BRCA1 prevents P_4-induced IRIS expression in PR^{+ve}-HME cells.

However, in orthotopic 1°-IRISOE tumors (**Figure 1Ha** and **1Hb**, for more details see Material and Methods and [52]), we discovered complete lack of BRCA1, and $pCBP_2$ proteins expression (**Figure 1Hc**, and **1Hd**, respectively). Additionally, IHC staining of a SEER breast cancer (BC) cohort (n=326) showed among 86% (n=281) BRCA1^{-ve} tumors (i.e., lack BRCA1 protein expression), 95% (n=267) were pCBP_2^{-ve} tumors (i.e. lack $pCBP_2$ protein, Ch Sq. 146.9, *P<0.00001*), and 83% (n=233) were IRISOE tumors (Ch sq. 61.1, *P<0.00001*) [52]. Similarly, in a sub-cohort of TNBC tumors (n=72), among 86% (n=62) BRCA1^{-ve} tumors (see example **Figure 1Ia** and **1Ia'**), 98% (n=61) were pCBP_2^{-ve} tumors (**Figure 1Ib** and **1Ib'**, Chi Sq. 56.2, *P<0.00001*), and 94% (n=58) were IRISOE tumors (Ch sq. 14.9, *P=0.000112*, see

example **Figure 1Ic** and **1Ic'**), suggesting IRISOE also suppressed BRCA1 (hence $pCBP_2$) expression in BC (especially TNBC) tumors. Indeed, meta-analysis using TCGA-BC cohorts confirmed high BRCA1+pCBP2+PGR expressors have improved OS (HR=0.62, *P=0.0026*, **Figure 1J**).

Taken together, we propose in PR^{+ve}-HME cells (perhaps in the mammary gland, as well), P_4-PR-B upregulates IRIS transcription directly or indirectly (e.g., through STAT5, see below, and **Figure 1K**). BRCA1 expressed specifically in these cells counteracts that by ubiquitylation-induced PR-B degradation [66], by enhancing PR-A expression (negatively affects PR-B [67]), or by inducing $pCBP_2$ expression [63]. Once induced, IRIS in a negative feedback loop reduces BRCA1 expression leading to sustained IRISOE in PR^{+ve}-cells (**Figure 1K**).

PRL induces IRIS expression in $PRLR^{+ve}$-HME cells

Unlike P_4 that transiently peaks in the mammary gland during pregnancy and early lactation, PRL is present at high-level during pregnancy and lactation (Figure S1B) [68-71]. In GFF-medium, PRL treatment of $PRLR^{+ve}$-HME cells for 24 h upregulated PRLR-LF (long form), and RANK in a biphasic pattern peaking at 1 μM, while had no effect on VDR expression (**Figure 2A**). PRL treatment upregulated IRIS protein and *mRNA* expression in $PRLR^{+ve}$-HME cells, also in a biphasic manner peaking at 0.5 μM (**Figure 2B** and **2C**). PRLR silencing in $PRLR^{+ve}$-HME cells (**Figure 2C**-inset) completely blunted PRL effect on *IRIS mRNA* expression (**Figure 2C**). Moreover, in GFF-medium, 100 μM of 573108 (prevents STAT5 SH2-dimerization) treatment of $PRLR^{+ve}$-HME cells blocked $STAT5^{Y694}$ phosphorylation (**Figure 2D**-inset), and significantly reduced PRL-induced *IRIS mRNA* expression (**Figure 2D**). In the absence of PRL treatment, 573108 had no effect on *IRIS mRNA* expression (Figure S2A). Moreover, in GFF-medium, PRL treatment (24 h) upregulated *IRIS mRNA* expression in $PRLR^{+ve}$- not $PRLR^{-ve}$-HME cells in the presence of vehicle not 10 μM IQDMA (prevents STAT5 phosphorylation, **Figure 2E**). PRLR-LF also signals through AKT and c-Src [72]. In GFF-medium, $PRLR^{+ve}$-HME cells were treated with 1 μM PRL in the presence of vehicle, 10 μM of IQDMA, LY294002 (inhibits PI3'K/AKT), or PP2 (inhibits c-Src) for 24 h. All drugs reduced PRL-induced IRIS and PRLR-LF proteins (**Figure 2F**), and *IRIS mRNA* (Figure S2B) expression. However, IQDMA effect was far superior to LY or PP2 effects (**Figures 2F**-upper, and S2B), suggesting PRL/PRLR-LF/STAT5 signaling activates IRIS transcription in $PRLR^{+ve}$-HME cells.

A positive feedforward loop between IRIS and PRL-PRLR-LF signaling in $PRLR^{+ve}$-HME cells

The above data suggest a feedforward loop between IRIS and PRLR signaling in $PRLR^{+ve}$-HME cells. However, while doxycycline (Dox)-treatment induced IRIS expression in HME clones carrying Dox-inducible IRIS allele, it did not affect PRLR-LF expression (**Figure 2G**). In contrast, compared to parental HME cells, the orthotopic 1°-IRISOE mammary tumor cell lines, IRIS293 and IRIS295 express 3-7-fold higher IRIS and PRLR-LF (**Figure 2H**). It is possible that this discrepancy is due to that the non-secreting HME-cells become PRL-secreting cells during tumor development (*cf.* **Figure 2A**). To evaluate that, we used ELISA to measure PRL level in condition media (CM) of 3 endogenously IRISOE-TNBC cell lines 231, 468, and MDA-MB-453 (453) [49, 50] expressing shCtl or shIRIS (see [54, 73]) grown in serum-free (SF)-media, and 2 ectopically IRISOE-TNBC cell lines, IRIS293 and IRIS295 also grown in GFF-media containing scrambled or IRIS inhibitory peptide (IRISpep [50, 56]). Compared to HME cells, all cell lines secreted high levels of PRL (**Figures 2I** and S2C), blocked by IRIS silencing in the endogenously IRISOE-TNBC cell lines (Figure S2C), and by IRISpep in the ectopically IRISOE-TNBC cell lines (**Figure 2I**), suggesting a positive feedforward loop between IRISOE and PRL/PRLR-LF signaling.

To reinforce this claim, we isolated total (T, by sonication), cytoplasmic (C), or nuclear/chromatin (N+Ch) proteins from 231 cells transfected with siCtrl or siIRIS for 72 h (to measure the effect of acute IRIS silencing, Figure S2D), or 453 and 468 cells expressing shCtrl or shIRIS (**Figure 2J**-inset). Compared to shCtrl-expressing cells, shIRIS-expressing cells contained higher levels of T-, C-, and N+Ch-total STAT3 levels (**Figure 2J**), and compared to si/shCtrl-expressing cells, si/shIRIS-expressing cells

contained higher levels of T-, C-, and N+Ch of p^{Y705}-STAT3 [74] (**Figures 2J** and S2D). In contrast, compared to shCtrl-expressing cells, shIRIS-expressing cells did not show significant change in the levels of T-, C-total STAT5, but significant lower levels of N+Ch-total STAT5 (**Figure 2J**), and compared to si/shCtrl-expressing cells, si/shIRIS-expressing cells contained significantly lower levels of T-, C-, and N+Ch of p^{Y694}-STAT5 [75] (**Figures 2J** and S2D). Additionally, compared to shCtrl-expressing cells, shIRIS cells contained significantly lower levels of T-, C-, and N+Ch-total AKT and $p^{S308T473}$-AKT (**Figure 2J**). Accordingly, compared to shCtrl-expressing cells, shIRIS-expressing cells contained significant lower levels of T-, C-, N+Ch-Cyclin D1 (**Figure 2J**), suggesting a local production and secretion of PRL from $PRLR^{+ve}$-IRISOE-TNBC cells maintains high IRIS and PRLR-LF expression to suppress p^{Y705}-STAT3-induced differentiation and enhances p^{Y694}-STAT5- and AKT-induced proliferation and survival in mammary cells (Figure S1A).

PRL promotes IRIS-induced proliferation, survival, and the TNBC-like phenotype (i.e., basal, stemness, and EMT) in $PRLR^{+ve}$-HME cells

To define the feedforward loop role in transforming mammary cells, *in vitro* and promoting BC (e.g., PABC), *in vivo* [50-52, 76, 77], we seeded 5000 siLuc- or siIRIS-transfected $PRLR^{+ve}$-HME cells for 48 h in GFF-media containing increasing concentrations of PRL for an additional 24 h. Cell count confirmed PRL increased siLuc-transfected cells number until a plateau starting at ~1 μM (**Figure 3A**-black line). In contrast, PRL had no effect at any of the concentrations tested in IRIS-silenced cells (**Figure 3A**-red line), suggesting the loop promotes proliferation in $PRLR^{+ve}$-HME cells.

Moreover, siLuc- or siIRIS-transfected (48 h) $PRLR^{+ve}$-HME cells were treated in GFF-media with vehicle, 1 or 2 μM of PRL for an additional 24 h. *RNAs* and proteins isolated from these cells were analyzed. Along with IRIS *mRNA* and protein (**Figure 3B**), PRL induced expression of the basal biomarkers, EGFR, CK5, and CK17 (**Figure 3C**), the stemness biomarkers, Oct4, Sox2, and Nanog [78-80] (**Figure 3D**), and the EMT biomarkers, CDH2, Slug, and Twist (**Figure 3E**) *mRNAs* and proteins in cells expressing not depleted from IRIS (**Figure 3B-E**). To further establish this, we performed mammosphere formation (MSF) assay (a hallmark of stemness/EMT in TNBC cells). Naïve HME or IRIS291 cells [54, 55] seeded in low-binding wells in GFF-media were treated with increasing concentrations of PRL in the presence of scrambled or IRISpep for a week (hormone and peptides changed every 2nd day). As previously shown [49, 50], vehicle-treated naïve HME cells formed organized, small size, non-invasive MSFs (**Figure 3Fa**), and exposure to PRL increased the size and the invasiveness of these MSFs in a concentration-dependent manner (**Figure 3Fb-d**), likely due to increasing IRIS expression. Indeed, compared to naïve HME, IRIS291 cells formed non-organized, larger, and invasive MSFs, exponentially increased by PRL treatment in a concentration-dependent manner in the presence of vehicle/scrambled peptide (**Figure 3Fe-h**), while organized, very small, and non-invasive MSFs at all PRL concentrations in the presence of IRISpep (**Figure 3Fi-l**). Identical results were obtained using IRIS293 cells (not shown), suggesting the loop promotes the TNBC-phenotype in $PRLR^{+ve}$-HME cells.

Finally, IHC staining of sections of orthotopic mammary tumors developed in athymic mice using 468 cells intratumorally treated with scrambled or IRISpep [50] showed that compared to scrambled (**Figure 3Ga**), IRISpep (**Figure 3Ge**) not only reduced tumor size by ~80% (see [50]), but prevented in addition to IRIS expression (compare **Figure 3Gf** to **3Gb**), Cyclin D1 (compare **Figure 3Gg** to **3Gc**), and survivin (compare **Figure 3Gh** to **3Gd**) expression. Identical results were obtained using MDA231 tumors (not shown), suggesting the loop promotes survival in $PRLR^{+ve}$-HME cells.

Taken together, we propose that *in vivo* (e.g., during pregnancy/early lactation), PRL locally produced and secreted or delivered from the pituitary gland triggers IRIS expression by activating PRLR-LF to inhibit STAT3-induced differentiation/apoptosis [81], and promote STAT5 (JNK and AKT)-induced proliferation/survival/TNBC-like phenotype [69-71, 81, 82] in $PRLR^{+ve}$-HME cells (**Figures 3H** and S1). IRISOE in turn upregulates PRLR-LF expression, and this positive feedforward loop triggers TNBC formation/progression. Noteworthy here, evidence against [83], and for [84, 85] PRLR-LF expression in TNBC cells exit.

RANKL upregulates IRIS expression in RANK^{+ve}-HME cells

RANKL promotes proliferation and survival in mammary epithelial cells [86]. To define whether this is through upregulating IRIS expression, we seeded RANK^{+ve}-HME cells in GFF-medium containing increasing concentration of RANKL for 24 h. RANKL treatment upregulated IRIS and RANK proteins (**Figure 4A**), and *IRIS mRNA* (**Figure 4B**) expression in cells expressing not lacking RANK expression (**Figure 4B**). However, unlike P_4 and PRL, RANKL had no effect on IRIS expression at lower concentrations (<1 μg/ml, **Figure 4A**).

In vivo, RANKL/RANK activates NF-κB, AKT, and JNK pathways in mammary epithelial cells [87]. In GFF-medium, we exposed RANK^{+ve}-HME cells to 2 μg/ml of RANKL *plus* vehicle, JSH-23 (inhibits NF-κB), LY, or SP600125 (inhibits JNK). The three drugs reduced the basal and RANKL-induced IRIS, RANK, and NF-κB expression to a different degrees (**Figure 4C**), with JNK inhibition showed the most dramatic effect on both the basal and the RANKL-induced expression of these proteins (**Figure 4C**). To further confirm, we treated RANK^{-ve}- and RANK^{+ve}-HME cells in GFF-medium with increasing concentrations of RANKL in the absence or presence of a c-Jun inactivating peptide for 24 h. As expected, RANKL increased *IRIS mRNA* expression in RANK^{+ve}-HME cells only in concentration-dependent manner starting at 1 μg/ml, and the c-Jun inhibitory peptide completely blocked this induction (**Figure 4D**), suggesting that RANKL/RANK/JNK/c-Jun signaling activates IRIS transcription in RANK^{+ve} cells.

Positive feedforward loop between IRIS and RANKL/RANK signaling triggers a TNBC-like phenotype in RANK^{+ve}-mammary cells

Compared to parental HME cells, all Dox-induced IRISOE clones showed high RANK protein expression (**Figure 4E**). Accordingly, IHC staining showed that compared to normal mammary glands [88], IRIS291 (as well as IRIS293) tumors [54, 73] express high level RANK in almost every cell in scrambled peptide-treated tumors, that decreased significantly in IRISpep-treated tumors (compare **Figure 4G** and **4G'** to **4F** and **4F'**, and data not shown). To test whether this is also due to locally produced and secreted RANKL, we again used ELISA to measure RANKL level in the CM of IRIS293 and IRIS295 grown in GFF-medium in the presence or absence of IRISpep (**Figure 4H**-inset). Both cell lines secreted high levels of RANKL in the presence of scrambled peptide, that was completely blocked by IRISpep (**Figure 4H**), suggesting a second positive feedforward loop between IRISOE and RANKL/RANK signaling in RANK^{+ve}-HME cells.

To determine whether this loop induces the TNBC-like phenotype in RANK^{+ve}-HME cells, we seeded these cells transfected with siLuc or siIRIS for 48 h in GFF-medium in the presence of vehicle, 1 or 2 μg/ml of RANKL for another 24 h. Along with *IRIS mRNA* (**Figure 4I**-left), RANKL induced expression of *CK5 and CK17 mRNAs* (**Figure 4I**-middle left), *Twist and Slug mRNAs* (**Figure 4I**-middle right), and *Oct4 and Sox2 mRNAs* (**Figure 4I**-right) expression in RANK^{+ve}-HME cells. Additionally, silencing IRIS in these cells blocked the induction of IRIS and all the other factors (**Figure 4I**). To reinforce these data further, we exposed naïve HME and IRIS293 cells [54, 55] in low-binding wells to GFF-media containing increasing concentrations of RANKL in the presence or absence of IRISpep for a week (cytokine and peptides changed every 2nd day). In the presence of vehicle, naïve HME cells formed organized, small size, non-invasive MSFs (**Figure 4Ja**), while IRIS293 cells formed unorganized, large size, and invasive MSFs (**Figure 4Je**). IRISpep alone negatively affected the growth of IRIS293 MSFs (**Figure 4Ji**). RANKL increased the size and the invasiveness of naïve HME MSFs in a concentration-dependent manner (**Figure 4Jb-d**), and exacerbated these events in IRIS293 MSFs also in a concentration-dependent manner (**Figure 4Jf-h**). Interestingly, unlike the situation with PRL (**Figure 3F**), IRISpep killed all IRIS293 in the presence of RANKL, even at the lowest concentration (**Figure 4Jj-l**). Identical results were obtained using IRIS291 cells.

Taken together, we propose that RANKL/RANK signaling upregulates IRIS expression in RANK^{+ve}-HME cells (perhaps in the mammary gland, *in vivo* as well) mostly through activating c-Jun/AP1 transcription complex. IRISOE enhances the TNBC-like phenotype in these cells, and the local production and secretion of RANKL from these cells, which maintains the

proposed positive feedforward loop and sustain IRISOE in these cells (**Figures 4K** and S1).

VD_3 suppresses IRIS expression in TNBC cells

When PRL level begins to drop in the mammary gland during late lactation, VD_3 level rises with signaling at a maximum during physiological involution (Figure S1B) [42]. VD_3 suppresses breast cancer cell growth, *in vitro*, and mammary tumors formation, *in vivo* [42, 89, 90]. IRIS-silencing or inactivation also suppresses TNBC cells growth, *in vitro* and tumor formation, *in vivo* [50, 54]. To investigate whether there is a connection between the two events, we seeded 3 VDR expressing TNBC cell lines, 231, 453, and 468, and one VDR^{-ve}-TNBC cell line, BT-549 [90] in SF (serum free) media containing vehicle, 1 or 2 μM VD_3 for 24 h. Compared to vehicle (see "0", **Figures 5A** and S3A), 1 μM of VD_3 was sufficient to completely abolish IRIS expression in all VDR^{+ve} cell lines (**Figures 5A** and S3A), while had no effect in the VDR^{-ve} cell line even at the highest concentration (2 μM, Figure S3A). To establish this further, we seeded VDR-silenced 231, 453, or 468 cells for 48 h (**Figures 5B**-insets, and S3B-inset) in SF-media containing vehicle, 1, or 2 μM VD_3 for another 24 h. VD_3 had no effect on *IRIS mRNA* expression in cells depleted from VDR (**Figures 5B**, S3B).

Negative feedback loop between IRIS and VD_3/VDR signaling suppresses the TNBC-like phenotype and promotes cell death in TNBC cells

Compared to parental HME cells, all Dox-induced IRISOE clones showed complete lack of VDR expression (**Figure 5C**). Moreover, compared to scrambled peptide treated IRIS291 (and IRIS293) tumors that lacked VDR expression (**Figure 5D**-left), IRISpep-treated tumors showed very high nuclear and cytoplasmic VDR expression (**Figure 5D**-right). Additionally, in SF-media, compared to vehicle, 231, 453, and 468 cells treated with increasing concentrations of VD_3 for 24 h showed significant increase in VDR expression in a concentration-dependent manner (at least in 231, and 468 cell lines, **Figures 5E**, S3C). Interestingly, the same treatment reduced PRLR-LF level in all cell lines, also in a concentration-dependent manner (**Figures 5E**, S3C), suggesting that VD_3/VDR signaling directly or indirectly suppresses IRIS transcription.

Next, equal number of 468 cells transfected with siLuc or siIRIS for 48 h were cultured in SF-medium containing 0, 1 or 2 μM VD_3 for an additional 24 h. VD_3 significantly decreased *IRIS mRNA* and protein expression (**Figure 5F**-upper left) along with CK5 and CK17 (**Figure 5F**-upper right), Twist and Slug (**Figure 5F**-lower left), and Oct4 and Sox2 (**Figure 5F**-lower right) *mRNAs* and proteins expression in concentration-dependent manner, in siLuc- not siIRIS-transfected cells (already lost in those cells [49, 50]). Interestingly, the effects on these biomarkers lagged after the effect on IRIS, suggesting a sequence of events. Identical results were obtained in 231 cells (data not shown). Furthermore, we cultured 231, 453, and 468 cells in ultra-low binding wells in SF-medium containing scrambled or IRISpep, and a suboptimal VD_3 concentration (0.5 μM) for a week (hormone and peptides changed every 2nd day). In the presence of scrambled peptide, all cell lines still formed unorganized, large size, and invasive MSFs in the presence of the suboptimal VD_3 concentration (**Figures 5G** and S3D). IRISpep blocked MSF formation in all cell lines, and induced their death by the suboptimal concentration of VD_3 (**Figures 5G** and S3D), suggesting a negative feedforward loop between IRISOE and VD_3/VDR signaling in TNBC cells.

To establish this further, we cultured the same number from these cell lines transfected with siLuc or siIRIS for 48 h in SF-media containing increasing concentrations of VD_3 followed by an additional 48 h. As expected, VD_3 treatment reduced survival of all cell lines transfected with siLuc not those transfected with siIRIS in a concentration-dependent manner (**Figures 5H**, S3E and S4). The IC_{50} for VD_3 in 453 was <1 μM (Figure S3E), in 468 was 1 μM, and in 231 cells was >1 μM (**Figure 5H**).

Taken together, we propose a negative feedback loop between IRISOE and VD_3/VDR signaling (perhaps on the transcriptional level) directly upregulates VDR or indirectly by downregulating PRLR expression. The reduction in IRIS expression by VD_3/VDR signaling inhibits the TNBC phenotype and facilitates their death by low VD_3 concentration.

Iris in the developing mammary gland

Like IRIS [50], Iris is expressed at low level in normal cell lines, HC11 (BALB/c) and C57MG

(C57BL/6), while at high level in TNBC cell lines, 4T1 (from a spontaneous BALB/c mammary tumor), and EO771 (from a spontaneous C57BL/6 mammary tumor) cell lines (**Figure 6A**-upper). Also, like IRIS [49, 50, 77, 91], Iris-silencing reduced Sox2 expression (**Figure 6A**-lower), decreased proliferation (i.e., BrdU incorporation, **Figure 6B**-left), and induced apoptosis (i.e., cleaved caspase 3/7, **Figure 6B**-right) in 4T1 and EO771 cells. More importantly, like IRIS-silenced cells [50, 55], Iris-silenced 4T1 or EO771 cells failed to develop orthotopic mammary tumors in BALB/c or C57BL/6 mice, respectively ([54], and data not shown), suggesting that despite the low homology between IRIS and Iris (~65% [48, 53, 92, 93]), the two proteins are functionally similar [48, 76, 91].

With this information at hand, we assessed the expression of Iris during the different phases of the mammary gland development. *RNA*s and proteins were isolated from whole glands from week (wk) 10 nulliparous/virgin (n=3), day (d) 15 pregnant (n=3), d3 lactating (n=3), d7 involuting (n=3), and d28 regressed (n=3) female C57BL/6 mice. Low levels of Iris *mRNA* and protein in nulliparous mice glands significantly increased in pregnant glands, remained high in lactating glands, but completely disappear in involuting glands, only to reappear at low levels again in regressed glands (**Figure 6C** and **6D**). To rule out these temporal changes are due to changes in epithelial:stromal cells composition during these stages, whole mammary glands from wk9 nulliparous (n=5), d10 pregnant (n=5), d6 lactating (n=5), d4 involuting (n=5), and d28 regressed (n=5) female C57BL/6 mice were dissociated into single-cell populations labeled with anti-mouse EpCAM antibody and FACS sorted. Again, low *Iris mRNA* level in $EpCAM^{+ve}$/luminal epithelial cells (progenitor and differentiated) from nulliparous glands was taken as 1-fold. Compared to that, we measured ~8-fold increase in Iris level in $EpCAM^{+ve}$-cells from pregnant glands, ~12-fold in $EpCAM^{+ve}$-cells from lactating glands, complete absence in $EpCAM^{+ve}$-cells from involuting glands, and ~1.1-fold in $EpCAM^{+ve}$-cells from regressed glands (**Figure 6E**). One-way ANOVA followed by Bonferroni post-hoc test confirmed the statistical significance even between multiple comparisons (*P*-value $=9.9922\times10^{-9}$, **Figure 6E**), suggesting that in mouse (perhaps in human as well) pregnancy increases Iris (IRIS) expression to promote replication/proliferation/survival and mammary glands expansion (Figure S1-step 1 and 2). These IrisOE (IRISOE) cells are specifically eliminated during involution, and replaced with $Iris^{low}$ ($IRIS^{low}$) during the mammary gland remodeling stage (Figure S1-step 3 and 4) [94].

Lactation vs. involution microenvironment effect on IRISOE vs. $IRIS^{low}$ cells

To define whether the involution microenvironment (with proven inflammation [95, 96]) differentially affects IRISOE vs. $IRIS^{-ve}$ cells, whole mammary glands isolated from d10-lactating (n=3), or d2-involuting (n=3) female BALB/c mice were flash-frozen, crushed by shaking with sterile steel balls, then their total proteins were extracted by sonication [97]. Early passage IRIS3 and IRIS5 clones (i.e., no prior Dox exposure) were exposed to Dox-free (-Dox) or Dox-containing (+Dox) media for 72 h (to induce IRIS expression, *cf.* **Figures 2G**, **4E**, and **5C**). Cells after that continued to grow in -Dox or +Dox containing media *plus* 500 µg of lactating or involuting extracts *plus* scrambled or IRISpep for an additional 24 h. Cells were then fixed, labelled with PI and cell cycle profile measured using FACS.

In lactating extracts, uninduced IRIS3 cells whether treated with scrambled peptide or IRISpep contained low level sub-G_1 (i.e., dying) cells, and normal cell cycle profile under both treatments (i.e., most cells in G_0/G_1-phase, low number in S-phase, and moderate number in G_2/M-phase, **Figure 6F**-left). Additionally, the number of 4N (tetraploid) cells was similar under both treatments (**Figure 6F**-left). Identical results were obtained using IRIS5 cells (Figure S5A). In lactating extracts, compared to uninduced IRIS3 treated with scrambled peptide, induced IRIS3 cells treated with scrambled peptide, while contained similar number of sub-G_1 cells, they showed lower G_0/G_1-phase cells (*P=0.0001*), higher S-phase (*P<0.0001*), and similar G_2/M-phase, and number of 4N cells (**Figure 6F**-right), supporting our previous conclusion that IRISOE promotes replication in mammary cells [48]. By contrast, induced IRIS3 cells in lactating extracts treated with IRISpep showed ~4-fold increase in sub-G_1 cells (*P=0.0013* vs. +Dox/Scram), high level

G_0/G_1-phase cells (*P=0.0005* vs. +Dox/Scram), lower-level S-phase cells (*P<0.0001* vs. +Dox/Scram), while G_2/M-phase, and the number of 4N cells remained unchanged (**Figure 6F**-right). Identical results were obtained using IRIS5 (Figure S5A), suggesting that IRIS activity is important for mammary cells replication (and transcription, see above) during lactation (and pregnancy), and that inhibiting this activity renders cells vulnerable to death during S-phase.

On the other hand, compared to uninduced IRIS3 cells in lactating extracts treated with scrambled peptide, those in involuting extracts contained 7-fold higher sub-G_1-phase cells (*P<0.00001*), lower G_0/G_1-phase (*P<0.00001*), and equal S-phase, G_2/M-phase, and number of 4N cells (compare **Figure 6G** to **6F**). Identical results were obtained using IRIS5 treated similarly (compare Figure S5B to S5A). Moreover, compared to uninduced IRIS3 treated with scrambled peptide in involuting extracts, those treated with IRISpep also showed high sub-G_1-phase, lower G_0/G_1-phase, and normal S-phase, G_2/M-phase, and low number of 4N cells (**Figure 6G**-left). Identical results were obtained using IRIS5 treated similarly (compared Figure S5B to S5A). Further, in involuting extracts, induced IRIS3 cells treated with scrambled peptide contained low number of sub-G_1-phase cells (*P<0.0001* vs. -Dox/Scram), higher G_0/G_1-phase (*P=0.0048* vs. -Dox/Scram), normal S-phase, and lower G_2/M-phase (*P<0.0001* vs. -Dox/Scram), but ~7-fold increase in the number of 4N cells (*P<0.0001* vs. -Dox/Scram, **Figure 6G**-right). Identical results were obtained using IRIS5 (Figure S5B). More importantly, induced IRIS3 treated with IRISpep in involuting extracts contained higher sub-G_1-phase (*P<0.0001* vs. +Dox/Scram), lower G_0/G_1-phase (*P=0.0161* vs. +Dox/Scram), and S-phase (*P=0.0965* vs. +Dox/Scram), higher G_2/M-phase (*P<0.0001* vs. +Dox/Scram), and very low number of 4N cells (*P<0.0001* vs. +Dox/Scram, **Figure 6G**-right). Identical results were obtained using IRIS5 (Figure S5B), suggesting that involution extracts triggers tetraploid (a precursor for aneuploid/aggressiveness) in IRISOE cells, which could be blocked in the presence of IRISpep, and these cells undergo apoptosis instead. These data support the need to eliminate IRISOE cells from the gland before involution (*cf.* **Figure 6C** and **6D**) to prevent the development of IRISOE tumors later.

The involution microenvironment promotes aneuploidy in IRISOE cells

We previously performed comparative genomic hybridization (CGH) on cells isolated from the 1° orthotopic IRISOE mammary tumors (IRIS291, IRIS292, and IRIS293) for genomic changes compared to their parental HME cells (n=5/each). This analysis identified low (deletion) and high (amplification) copy numbers in these tumors (Figure S6A). We chose 11 genes located in areas showed deletion in the above CGH (JAK1 [1q31], MOB1 [2q13], MFN1 [3q26], STAP1 [4q13], SPZ1 [5q14], TESTIN [7q31], PPP3R2 [9q31], KCTD14 [10q14], GNG2 [14q22], CDYL2 [16q2LGR4 [11p14], 3], FGS4 [Xq12]), and 11 genes located in areas showed amplification in the above CGH (ST6GAL2 [2q12], LPP [3q27], FGFR1 [8p11], TLE1 [9q21], KCNMA1 [10q22], ARF6 [14q21], CX3CL1 [16q21], SUZ12 [17p11], NDC80 [18p11], PAK5 [20p12]). Interestingly, several of these areas are proven alterations in TNBC tumors [16, 25, 98-101]. Indeed, TCGA analysis of TNBC patient cohorts showed high expressors of the genes located in the deleted areas experience lower risk of distant metastasis free survival (DMFS, Figure S6B), and high expressors of the genes located in the amplified areas (especially, LPP and ARF6, the rest showed trends, but significance was low, not shown) experience higher risk of RFS (Figure S6C).

To define whether tetraploid induced in IRISOE cells by the involution extracts progress to aneuploidy, we reasoned that if IRISOE is the common denominator between the two events it is possible to use these surrogates to verify whether involution induces aneuploidy in mammary cells with IRISOE. As an added bounce, this analysis could inform us whether a recurrent genomic alteration could be induced by IRISOE cells even if the starting points are different.

Similar cultures of IRIS-Dox/Scram, +Dox/Scram, and +Dox/IRISpep in the presence of involution extracts (n=5/each) were continued for an additional 72 h. Using RTqPCR primers that amplify the transcripts mentioned above, we showed that the expression of the genes in

the deleted areas are expressed at high level in uninduced IRIS3 exposed to involution extracts *plus* scrambled peptide (*cf.* **Figure 6H1**), decreased in induced cells similarly treated (*cf.* **Figure 6H2**), and at high levels in induced cells in the presence of involution extracts *plus* IRISpep (*cf.* **Figure 6H3**). In contrast, the genes in the amplified areas were expressed at low level in uninduced IRIS3 exposed to involution extracts *plus* scrambled peptide (*cf.* **Figure 6I1**), increased in induced cells similarly treated (*cf.* **Figure 6I2**), and at high levels in induced cells in the presence of involution extracts *plus* IRISpep (*cf.* **Figure 6I3**).

Taken together, we propose that involution microenvironment triggers aneuploidy in mammary cells overexpressing IRIS, and support the need to downregulate IRIS before the onset of involution to prevent the formation an aggressive IRISOE-TNBC-PABC 2-5 years after full term pregnancy.

Forced vs. physiological involution: a road to the development of aggressive IRISOE-BC

Several studies have documented a 25%-50% lower risk of BC in parous women who have breastfed their infants for >6 months relative to parous women who have never breastfed their infants [102-106]. In mice, the physiological weaning occurs at ~3 weeks of lactation, while forced weaning could be induced by separating pubs right after birth or shortly after lactation starts. To model the effect of forced vs. physiological involution on Iris (perhaps IRIS, as well) expression and the physiology of the mammary gland, we impregnated BALB/c mice (n=10). At birth, mice were randomized into 2 groups (n=5ea) that were allowed to nurse for 3 weeks (**Figure 6J**-left) or for 5 days only (**Figure 6K**-left). In both situation, mice recovered for 6 days (enough to remove all secretory epithelium [107]) underwent each protocol a total of 3 times (**Figure 6J** and **6K**-lefts). At the end, whole mammary glands were collected from all mice, dissociated into single cell preparations, labeled with anti-mouse EpCAM antibody, and FACS sorted. $EpCAM^{+ve}$/mammary epithelial cells from mice underwent forced involution contained 8-9-fold higher *Iris mRNA* than mice underwent physiological involution (compare **Figure 6K**-right to **Figure 6J**-right).

To relate this to aggressiveness gene signature, we selected 6 known involution inhibitor (IRF-1, SREBF-1, Sim2s, ADIPOQ, IGF-1, and JAK2, hereafter inhibitors) and 6 known involution activators (IGFBP5, cEBPd, LIF, FasL, ATF4, and cathepsin L, hereafter activators) in the mouse and other species [95, 107-109] to determine their levels in the mice cohort above. Surprisingly, we detected high expression levels of the involution activators, and low expression levels of the involution inhibitors in gland from forced involuting mice (**Figure 6L**). TCGA analysis showed that high expressors TNBC patients of the involution inhibitors, IRF-1, SREBF1, IGF-1, and JAK2 are at lower risk of RFS (Figure S7A), while high expressors TNBC patients of the involution activators, c-EBPd and IGFBP5 are at higher risk of DMFS (Figure S7B). In contrast, we detected low expression levels of the involution activators, and high levels of the involution inhibitors in the glands from physiologically involuting mice (**Figure 6L**). Recently, we showed in mice model, under inflammatory and/or hypoxic microenvironment IRISOE cells thrive and develop into metastatic TNBC tumors [54, 55, 73].

Taken together, we propose that prolonged breastfeeding (3 weeks in mice, >12 months in women [104, 110-115]), IrisOE (perhaps IRISOE) cells have all terminally differentiated, including reducing Iris (IRIS) expression leading to their death during physiological involution. Following no breastfeeding or short-term breastfeeding, the mammary glands still contain large number of IrisOE (IRISOE) that could thrive in the inflammatory microenvironment induced by forced involution [96, 108] develop into TNBC [115] shortly after full-term pregnancy.

Human data confirm a direct relationship between lack of breastfeeding and formation of aggressive IRISOE-BCs

To test the hypothesis that lack of breastfeeding induces retention of IRISOE cells within the mammary gland that progress into aggressive breast cancer later, we analyzed a breast cancer cohort (n=49) consisting of 24 patients with $IRIS^{-ve}$ tumors, and 25 patients with IRISOE tumors. Age, menopausal status, and tumor grade were not risk factors for the development of IRISOE tumors (**Figure 7A**). ER, PR or

A

	IRIS-negative (n=24)		IRIS-overexpressing (n=25)		Chi sq.	*p*-value
Age	<40	>40	<40	>40		
	2	22	6	19	2.2	*0.13801*
Menopausal	Pre	Post	Pre	Post		
	8	16	11	14	0.6	*0.44364*
Grade	I+II	III+IV	I+II	III+IV		
	19	5	15	10	1.1	*0.28884*
ER	Negative	Positive	Negative	Positive		
	12	12	8	17	1.6	*0.20000*
PR	Negative	Positive	Negative	Positive		
	11	13	10	15	0.1	*0.76075*
HER2	Negative	Positive	Negative	Positive		
	20	4	19	6	0.9	*0.34187*
Clinical diagnosis	Locally Advanced	IBC	Locally Advanced	IBC		
	14	10	6	19	6.0	*0.01451*
Clinical response	No	Yes	No	Yes		
	1	18	11	14	8.2	*0.0043*
Parity	No	Yes	No	Yes		
	2	22	2	23	0	*1*
Lactation	No	Yes	No	Yes		
	3	19	19	4	23.5	*>0.00001*
Progression	No	Yes	No	Yes		
	20	4	7	18	15.2	*>0.00001*

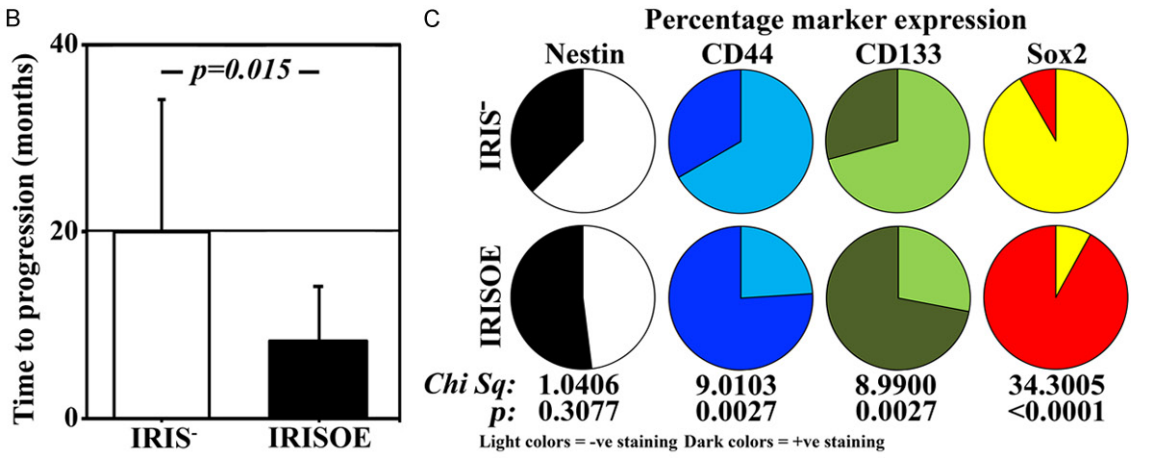

Figure 7. Human data support IRISOE is associated with the worse outcomes, shorter time to progression, stem-like phenotype, and lack of breastfeeding in aggressive BCs. (A) Univariate Chi-square test to determine the association between IRISOE and clinicopathological characteristics, parity, lactation, and progression. (B) The average time to progression in the patients in (A). (C) The percentage of negative stained (light colors) or positive stained (dark colors) IBC tumors with the indicated markers.

HER2 expressions were not significantly different between the two groups (perhaps due to the small sample size, **Figure 7A**). In sharp contrast, however, more IRISOE patients were diag-

nosed with an aggressive inflammatory breast cancer (IBC, Chi. sq. 6.0, *P=0.01451*, **Figure 7A**). Although rare (<5% of all breast cancers diagnosed in the USA), IBC is the most aggressive locally advance ductal carcinomas that develop from cells lining the milk ducts, often progress rapidly, diagnosed as stage III or IV disease, and is high in African American and obese women [116]. Accordingly, more IRISOE patients within this cohort showed chemotherapy-resistance compared to patients with $IRIS^{low}$ tumors (Chi. sq. 8.2, *P=0.0043*, **Figure 7A**). More importantly, while parity was not a risk factor in either group, breastfeeding was a strong inducer of IRISOE-IBC tumors. Indeed, in the $IRIS^{low}$ group only 3 patients (14%) never breastfed their infants, whereas in the IRISOE group, 19 patients (83%) never breastfed their infants (Chi. sq. 23.5, *P>0.00001*, **Figure 7A**). This correlated to only 5 $IRIS^{low}$ patients (21%) developed metastasis, while 20 IRISOE (84%) developed metastasis (Chi. sq. 17.2, *P=0.000034*, **Figure 7A**). Importantly, the majority of the IRISOE patients that developed IBC tumors after lack of breastfeeding were those developed metastasis. Additionally, time to progression was much shorter in the IRISOE patients compared to the $IRIS^{-ve}$ patients (8.3±5.8 months vs. 19.9±14.3 months, *P=0.015*, **Figure 7B**). Finally, the expression of 4 well known stemness biomarkers, nestin [117], CD44 [118], CD133 [119], Sox2 [120, 121] associated with aggressive BC formation was analyzed. $Nestin^{+ve}$ tumors were not different between IRISOE group compared to $IRIS^{-ve}$ group (37% vs. 52%, Chi. sq.=1.04, *P=0.3077*, **Figure 7C**-black and white). However, the $CD44^{+ve}$ tumors (76% vs. 33%, Chi. Sq.=9.0103, *P=0.0027*, **Figure 7C**-light and dark blue), the $CD133^{+ve}$ tumors (72% vs. 29%, Chi. Sq.=8.99, *P=0.0027*, **Figure 7C**-light and dark green), and most importantly, the $Sox2^{+ve}$ tumors (92% vs. 8%, Chi. Sq.=34.3005 *P< 0.00001*, **Figure 7C**-yellow and red) were over-represented in the IRISOE group.

Discussion

In the mammary gland, the specification of immature progenitors into mature differentiated cells is driven primarily by P_4, PRL, and RANKL [69]. During pregnancy, the mammary gland contains luminal PR^{+ve} (sensor) cells, luminal PR^{-ve} (responder) cell, and basal PR^{-ve}-cells. Our FACS analysis showed HME cell lines contain a population ~25% that express ER, PR, and PRLR, perhaps corresponding to the sensor cells (Figure S8A-blue), another ~25% express PRLR and RANK, perhaps corresponding to a responder type I cells (Figure S8A-green), and a 3rd ~50% express RANK only, perhaps corresponding to responder type II and basal cells (Figure S8A-pink).

As reported earlier [71, 122], P_4 activated transcription and secretion of RANKL, Wnt4, and RSPO1 from $PR^{+ve}/PRLR^{+ve}$-HME cells. It is possible that these ligands activate IRIS transcription in cell population that express their cognate receptor(s) within the mammary gland (Figure S8A). It is interesting that P_4 did not affect PRLR-LF or RANK expression in the $PR^{+ve}/PRLR^{+ve}$-HME cells. However, as earlier reported [60], P_4 enhanced VDR expression in $PR^{+ve}/PRLR^{+ve}$-HME cells. Based on these data, we propose that these cells are the most vulnerable to death by VD_3 effect (Figure S8). P_4 also upregulated IRIS on the protein and the *mRNA* levels, suggesting transcriptional activation. However, since IRISOE is detected mainly in TNBC cells [49, 50, 54, 55], it is unlikely that PR-B binds to the promoter of IRIS. Instead, we propose that PR-B alone or in cooperation with PRL/PRLR activates IRIS transcription in this $PR^{+ve}/PRLR^{+ve}$-HME cell population through activating JAK2/STAT5, c-Src/MAPK, or PI3'K/AKT [8, 22, 50, 76, 123] (**Figures 1K** and S8A). A limitation of the current study is that IRIS promoter has yet to be identified. Thus, these possibilities remain to be experimentally tested.

It is interesting that BRCA1 protein expression is confined to the PR^{+ve} cells. BRCA1 inhibits PR activity and blocks progesterone-stimulated gene expression and cell proliferation, in part, by preventing PR from binding to the PRE and by promoting the formation of a corepressor complex rather than a coactivator complex [124]. Other mechanisms to inhibit PR effect, including promoting ubiquitination of unliganded or liganded PR has been recently proposed for BRCA1 [66]. Finally, recent evidence also showed that BRCA1 enhances PR-A expression, which inhibits PR-B (the form studied herein) [67]. The fact that depleting BRCA1 from $PR^{+ve}/PRLR^{+ve}$-HME cells further upregulated IRIS in response to P_4 confirms BRCA1

negative role on PR. However, we previously showed that BRCA1 directly targets *IRIS mRNA* for degradation by upregulating expression of several *mRNA-3'-UTR* binding and degrading proteins, e.g., AUF-1 and $pCBP_2$ [63]. The fact that in IRISOE-TNBC tumors in women or mice, BRCA1 and $pCBP_2$ expressions were lacking, and that $pCBP_2$+PGR+ BRCA1 expressors showed improved OS support the existence of a delicate balance between BRCA1/$pCBP_2$ on one hand and PR-B/IRIS on the other that maintains proliferation and survival in the PR^{+ve}/$PRLR^{+ve}$ population of mammary cells in the gland. It is possible that, at least some of P_4/PR-B effects, e.g., proliferation [69-71] during pregnancy and lactation [8] (Figure S1-step 1 and 2) could be driven by P_4/PR-B-induced IRIS expression in these PR^{+ve} epithelial cell directly, as with RANKL or indirectly (e.g., through activating STAT5 [125]), as with RSPO1 by promoting autocrine activation of ErbB4 by EGF-like ligand (EGF, NRG1, or AREG) secreted by these PR^{+ve} cells [56, 62].

Our studies are consistent with recent reports showing PRL induces expression of PRLR-LF in a STAT5-dependent manner during differentiation of epididymal preadipocytes in the rat [126]. To our knowledge, we are the first to show that PRL induces RANK and IRIS expression also in a STAT5-dependent manner. The close correlation between PRL-induced IRIS and PRLR-LF expression in this population suggests that while IRIS is a downstream target of PRLR-LF, PRLR-LF could also be a downstream target of IRISOE. The fact that PRL triggered IRIS expression, and that IRISOE inhibits STAT3 [69, 127, 128], while activates STAT5 and AKT in the $PRLR^{+ve}$ population suggests that once overexpressed, IRIS maintains its own expression at high level in the absence of PRL. We propose that PRL-induced IRISOE triggers $PRLR^{+ve}$-HME cells proliferation, survival and the TNBC-like phenotype, during pregnancy/early lactation through activation of JAK2/STAT5 directly or by activating c-Src/JNK or PI3'K/AKT signaling [129, 130] (**Figure 3H**), in part by stimulating JAK2-STAT5 [69-71, 81, 82] (as well as c-Src-JNK, or PI3'K-AKT) signaling. IRISOE could also inhibit differentiation/apoptosis in this population, in part by suppressing STAT3 expression/activation [81]. Indeed, in the mammary gland, STAT5 is activated during lactation, while STAT3 during involution and the two inhibit each other's function [74, 131]. The positive feedforward between IRISOE and PRLR expression and signaling in $PRLR^{+ve}$-population perhaps is involved in TNBC formation/progression. Evidence against [83], and for [84, 85] expression of PRLR-LF in TNBC cells exist. To our knowledge, we are the first to show that PRL-treatment activates the TNBC-phenotype in the $PRLR^{+ve}$ population, including promoting the basal, EMT, and stemness gene signatures. The fact that this requires IRISOE suggests that this population if maintained within the mammary gland after full term pregnancy could become precursors for a TNBC tumor (Figure S8A-green). Indeed, only in the presence of IRISpep, PRL-induced MSFs was completely blocked (**Figure 3F**).

Upregulating IRIS activates RANK expression in responder type II cells [69]. RANK is expressed specifically on normal mammary stem cells, common progenitors, luminal progenitors, and cancer stem cells. If true, this suggests that constitutive RANK expression driven by IRISOE in immature mammary cells could disrupt mammary cell fate leading to tumorigenesis [32]. Consistent with that we found that IRISOE-TNBC tumors overexpress RANK (**Figure 4F**, **4G'**), and RANKL-treated cells show the TNBC-phenotype (**Figure 4I**). The fact that they require IRISOE to do so, suggests that this population as well if maintained within the mammary gland after full term pregnancy could become precursors for a TNBC tumor (Figure S8A-pink). Indeed, only in the presence of IRISpep, RANKL-induced MSFs was completely blocked (**Figure 4J**). Taken together suggest RANKL, Wnt4, and RSPO1 locally produced from $RANK^{+ve}$ or PR^{+ve} cells signaling through RANK, frizzled and LGR4/5 receptors could induce IRIS expression, the proliferation, survival, and the TNBC-like phenotype in the $RANK^{+ve}$ subpopulation of the mammary gland in a JNK/c-Jun-, NF-κB- and AKT-dependent manner (**Figures 4K** and S8A).

Upon cessation of breastfeeding, milk stasis or VDR activation by VD_3, downregulation of IRIS could activate STAT3 to antagonize STAT5 and AKT activities leading to epithelial cells death [69, 127, 128]. Our data are consistent with recent observations showing P_4/PR tran-

scriptionally induces VDR expression in T cells, which makes them highly sensitive to VD_3, even when its level is suboptimal [60]. A similar situation may occur in the mammary gland during pregnancy. P_4 upregulates the expression of IRIS and VDR, simultaneously. In the absence of VD_3 during pregnancy/early lactation, IRISOE effect dominates leading to induction of proliferation and survival (Figure S1B). During late lactation, before the physiological involution an increase in VD_3 level within the mammary gland could activate VDR signaling to directly downregulates IRIS expression or indirectly by down-regulating PRLR or upregulating VDR expression (Figure S1B). This could allow for terminal differentiation of mammary cells to occur, which allows their death by the inflammatory microenvironment during physiological involution [132] (*cf.* Figure S1A and S1B). Epidemiological and experimental evidence support the protective role of VD_3 against breast cancer, through regulating gene transcription [133, 134]. Decreased sunlight exposure diminishes VD_3 production by the skin, which is correlated with higher breast cancer incidence and mortality. TNBC patients display the lowest levels of VD_3 [135, 136]. Compared to wild-type counterparts, *Vdr* knockout female mice display more extensive ductal elongation and branching [42, 43]. In these mice, mammary gland regression after weaning was delayed due to a significant reduction in apoptosis in the epithelial cell compartment [42]. It is possible that the downregulation of IRIS by VD_3/VDR helps prepare mammary epithelial cells to death by the pro-inflammatory and hypoxic microenvironment during the physiological involution (Figure S1B).

Pregnancy-associated breast cancer (PABC) is diagnosed within 2-5 years following full-term childbirth. It is generally presenting at an advanced stage and has a poor prognosis [137]. Several large studies speculated that involution rather than pregnancy initiates this disease [106, 110, 112-114, 138-142]. We expand these speculations based on our current studies and argue that during no/short-term lactation, forced involution starts even-though the mammary gland still contains many IRISOE-TNBC-like cells. These cells thrive in the harsh inflammatory and hypoxic microenvironment induced by the forced involution to become TNBC tumor cells after full-term pregnancy (Figure S8B) [49, 54, 55]. In contrast, during physiological involution after an extended period of breastfeeding (several large-scale epidemiological and clinical studies put it between 12 and 18 months) was associated with >50% PABC risk reduction (OR, 0.51; 95% CI, 0.45 to 0.58) [104, 142, 143]. During this long-term lactation, the mammary gland matures, and all mammary epithelial cells terminally differentiate (in part by downregulating IRIS in a VD_3-dependent manner). $IRIS^{low}$/terminally differentiated cells are specifically targeted for death by the inflammatory/hypoxic microenvironment during physiological involution [111] (Figure S8B).

Conclusions

The expansion of the mammary gland during pregnancy that continues during lactation correlated well with the surge in Iris (possibly IRIS) expression in the mammary gland (Figure S1B). This upregulation in IRIS expression exacerbates the proliferation/survival required in the mammary gland during pregnancy and lactation. However, the upregulation in IRIS also exacerbates the TNBC-like phenotype in normal mammary epithelial cells. Extending the lactation period to ≥12 months allows for a surge in VD_3/VDR/STAT3, MFG-E8/STAT3, or IGFBP5 [144, 145] signaling, which all decrease IRIS expression, and promote mammary epithelial cells terminal differentiate (**Figure 1**) [110, 112-114, 141, 143, 146]. Terminally differentiated cells are vulnerable to the pro-inflammatory microenvironment [91, 147] induced during physiological involution [148]. Our data support a model in which IRIS expression is strictly controlled during pregnancy. Cells that overexpress IRIS during pregnancy/lactation through effects of hormones such as P4, PRL, and RANKL must die out during involution in response to VD_3 surge and to be replaced by $IRIS^{low}$ cells. This suggests that IRISOE could be a useful diagnostic biomarker for breast cancer that may develop 2-5 years after a full-term pregnancy and a valid target to treat these tumors.

Acknowledgements

The authors would like to thank Dr. Abeer Bahnessy, NCI, Cairo, Egypt for communicating the unidentified breast cancer cohort data presented to us. Wael is Dr. Lawrence & Mrs. Bo

Hing Chan Tseu, American Cancer Society Research Scholar. This research is supported by a National Cancer Institute grant R01 CA194447. The funding body had no role in the design of the study and collection, analysis, interpretation of data, and writing the manuscript.

Disclosure of conflict of interest

None.

Address correspondence to: Dr. Wael M ElShamy, Breast Cancer Program, San Diego Biomedical Research Institute, UC San Diego Health System, 3525 John Hopkins Ct, San Diego, CA 92121, USA. Tel: 858-200-7195; Fax: 858-445-9830; E-mail: welshamy@sdbri.org

References

[1] Halperin J, Dorfman VB, Fraunhoffer N and Vitullo AD. Estradiol, progesterone and prolactin modulate mammary gland morphogenesis in adult female plains vizcacha (lagostomus maximus). J Mol Histol 2013; 44: 299-310.

[2] Binart N, Helloco C, Ormandy CJ, Barra J, Clement-Lacroix P, Baran N and Kelly PA. Rescue of preimplantatory egg development and embryo implantation in prolactin receptor-deficient mice after progesterone administration. Endocrinology 2000; 141: 2691-2697.

[3] Aupperlee MD, Drolet AA, Durairaj S, Wang W, Schwartz RC and Haslam SZ. Strain-specific differences in the mechanisms of progesterone regulation of murine mammary gland development. Endocrinology 2009; 150: 1485-1494.

[4] Wang S, Counterman LJ and Haslam SZ. Progesterone action in normal mouse mammary gland. Endocrinology 1990; 127: 2183-2189.

[5] Skarda J, Fremrová V and Bezecný I. Progesterone alone is responsible for stimulation of the growth of ducts and of mammary alveolar structures in mice. Endocrinol Exp 1989; 23: 17-28.

[6] Atwood CS, Hovey RC, Glover JP, Chepko G, Ginsburg E, Robison WG and Vonderhaar BK. Progesterone induces side-branching of the ductal epithelium in the mammary glands of peripubertal mice. J Endocrinol 2000; 167: 39-52.

[7] Lee HJ and Ormandy CJ. Interplay between progesterone and prolactin in mammary development and implications for breast cancer. Mol Cell Endocrinol 2012; 357: 101-107.

[8] Horseman ND. Prolactin and mammary gland development. J Mammary Gland Biol Neoplasia 1999; 4: 79-88.

[9] Brisken C, Kaur S, Chavarria TE, Binart N, Sutherland RL, Weinberg RA, Kelly PA and Ormandy CJ. Prolactin controls mammary gland development via direct and indirect mechanisms. Dev Biol 1999; 210: 96-106.

[10] Berryhill GE, Trott JF and Hovey RC. Mammary gland development--it's not just about estrogen. J Dairy Sci 2016; 99: 875-883.

[11] Mol JA, Lantinga-van Leeuwen I, van Garderen E and Rijnberk A. Progestin-induced mammary growth hormone (GH) production. Adv Exp Med Biol 2000; 480: 71-76.

[12] Queiroga FL, Pérez-Alenza MD, Silvan G, Peña L, Lopes CS and Illera JC. Crosstalk between GH/IGF-I axis and steroid hormones (progesterone, 17beta-estradiol) in canine mammary tumours. J Steroid Biochem Mol Biol 2008; 110: 76-82.

[13] Oguri H, Suganuma N, Kikkawa F, Ishihara Y, Seo H, Matsui N and Tomoda Y. Regulation of prolactin gene expression during early pregnancy in rats. Endocrinol Jpn 1989; 36: 395-401.

[14] Hovey RC, Trott JF, Ginsburg E, Goldhar A, Sasaki MM, Fountain SJ, Sundararajan K and Vonderhaar BK. Transcriptional and spatiotemporal regulation of prolactin receptor mRNA and cooperativity with progesterone receptor function during ductal branch growth in the mammary gland. Dev Dyn 2001; 222: 192-205.

[15] Goldhar AS, Vonderhaar BK, Trott JF and Hovey RC. Prolactin-induced expression of vascular endothelial growth factor via Egr-1. Mol Cell Endocrinol 2005; 232: 9-19.

[16] Seagroves TN, Lydon JP, Hovey RC, Vonderhaar BK and Rosen JM. C/EBPbeta (CCAAT/enhancer binding protein) controls cell fate determination during mammary gland development. Mol Endocrinol 2000; 14: 359-368.

[17] Nagata C, Wada K, Nakamura K, Hayashi M, Takeda N and Yasuda K. Associations of body size and reproductive factors with circulating levels of sex hormones and prolactin in premenopausal Japanese women. Cancer Causes Control 2011; 22: 581-588.

[18] Eliassen AH, Tworoger SS and Hankinson SE. Reproductive factors and family history of breast cancer in relation to plasma prolactin levels in premenopausal and postmenopausal women. Int J Cancer 2007; 120: 1536-1541.

[19] Yu MC, Gerkins VR, Henderson BE, Brown JB and Pike MC. Elevated levels of prolactin in nulliparous women. Br J Cancer 1981; 43: 826-831.

[20] Tworoger SS and Hankinson SE. Prolactin and breast cancer risk. Cancer Lett 2006; 243: 160-169.

[21] Tworoger SS, Sluss P and Hankinson SE. Association between plasma prolactin concentra-

tions and risk of breast cancer among predominately premenopausal women. Cancer Res 2006; 66: 2476-2482.
[22] Yu J, Xiao F, Zhang Q, Liu B, Guo Y, Lv Z, Xia T, Chen S, Li K, Du Y and Guo F. PRLR regulates hepatic insulin sensitivity in mice via STAT5. Diabetes 2013; 62: 3103-3113.
[23] Langenheim JF and Chen WY. Development of a novel ligand that activates JAK2/STAT5 signaling through a heterodimer of prolactin receptor and growth hormone receptor. J Recept Signal Transduct Res 2009; 29: 107-112.
[24] Sakamoto K, Creamer BA, Triplett AA and Wagner KU. The Janus kinase 2 is required for expression and nuclear accumulation of cyclin D1 in proliferating mammary epithelial cells. Mol Endocrinol 2007; 21: 1877-1892.
[25] Shillingford JM, Miyoshi K, Robinson GW, Grimm SL, Rosen JM, Neubauer H, Pfeffer K and Hennighausen L. Jak2 is an essential tyrosine kinase involved in pregnancy-mediated development of mammary secretory epithelium. Mol Endocrinol 2002; 16: 563-570.
[26] Tan D, Chen KE, Deng C, Tang P, Huang J, Mansour T, Luben RA and Walker AM. An N-terminal splice variant of human Stat5a that interacts with different transcription factors is the dominant form expressed in invasive ductal carcinoma. Cancer Lett 2014; 346: 148-157.
[27] Li H, Ahonen TJ, Alanen K, Xie J, LeBaron MJ, Pretlow TG, Ealley EL, Zhang Y, Nurmi M, Singh B, Martikainen PM and Nevalainen MT. Activation of signal transducer and activator of transcription 5 in human prostate cancer is associated with high histological grade. Cancer Res 2004; 64: 4774-4782.
[28] Schramek D, Leibbrandt A, Sigl V, Kenner L, Pospisilik JA, Lee HJ, Hanada R, Joshi PA, Aliprantis A, Glimcher L, Pasparakis M, Khokha R, Ormandy CJ, Widschwendter M, Schett G and Penninger JM. Osteoclast differentiation factor RANKL controls development of progestin-driven mammary cancer. Nature 2010; 468: 98-102.
[29] Chakrabarti R, Wei Y, Romano RA, DeCoste C, Kang Y and Sinha S. Elf5 regulates mammary gland stem/progenitor cell fate by influencing notch signaling. Stem Cells 2012; 30: 1496-1508.
[30] Choi YS, Chakrabarti R, Escamilla-Hernandez R and Sinha S. Elf5 conditional knockout mice reveal its role as a master regulator in mammary alveolar development: failure of Stat5 activation and functional differentiation in the absence of Elf5. Dev Biol 2009; 329: 227-241.
[31] Lee HJ, Gallego-Ortega D, Ledger A, Schramek D, Joshi P, Szwarc MM, Cho C, Lydon JP, Khokha R, Penninger JM and Ormandy CJ. Progesterone drives mammary secretory differentiation via RankL-mediated induction of Elf5 in luminal progenitor cells. Development 2013; 140: 1397-1401.
[32] Pellegrini P, Cordero A, Gallego MI, Dougall WC, Munoz P, Pujana MA and Gonzalez-Suarez E. Constitutive activation of RANK disrupts mammary cell fate leading to tumorigenesis. Stem Cells 2013; 31: 1954-1965.
[33] Fata JE, Kong YY, Li J, Sasaki T, Irie-Sasaki J, Moorehead RA, Elliott R, Scully S, Voura EB, Lacey DL, Boyle WJ, Khokha R and Penninger JM. The osteoclast differentiation factor osteoprotegerin-ligand is essential for mammary gland development. Cell 2000; 103: 41-50.
[34] Sigl V, Owusu-Boaitey K, Joshi PA, Kavirayani A, Wirnsberger G, Novatchkova M, Kozieradzki I, Schramek D, Edokobi N, Hersl J, Sampson A, Odai-Afotey A, Lazaro C, Gonzalez-Suarez E, Pujana MA, Cimba F, Heyn H, Vidal E, Cruickshank J, Berman H, Sarao R, Ticevic M, Uribesalgo I, Tortola L, Rao S, Tan Y, Pfeiler G, Lee EY, Bago-Horvath Z, Kenner L, Popper H, Singer C, Khokha R, Jones LP and Penninger JM. RANKL/RANK control Brca1 mutation. Cell Res 2016; 26: 761-774.
[35] Asselin-Labat ML, Vaillant F, Sheridan JM, Pal B, Wu D, Simpson ER, Yasuda H, Smyth GK, Martin TJ, Lindeman GJ and Visvader JE. Control of mammary stem cell function by steroid hormone signalling. Nature 2010; 465: 798-802.
[36] Fu NY, Nolan E, Lindeman GJ and Visvader JE. Stem cells and the differentiation hierarchy in mammary gland development. Physiol Rev 2020; 100: 489-523.
[37] Nolan E, Vaillant F, Branstetter D, Pal B, Giner G, Whitehead L, Lok SW, Mann GB, Rohrbach K, Huang LY, Soriano R, Smyth GK, Dougall WC, Visvader JE and Lindeman GJ. RANK ligand as a potential target for breast cancer prevention in BRCA1-mutation carriers. Nat Med 2016; 22: 933-939.
[38] Cantrell MA, Ebelt ND, Pfefferle AD, Perou CM and Van Den Berg CL. c-Jun N-terminal kinase 2 prevents luminal cell commitment in normal mammary glands and tumors by inhibiting p53/Notch1 and breast cancer gene 1 expression. Oncotarget 2015; 6: 11863-11881.
[39] Liu S, Ginestier C, Charafe-Jauffret E, Foco H, Kleer CG, Merajver SD, Dontu G and Wicha MS. BRCA1 regulates human mammary stem/progenitor cell fate. Proc Natl Acad Sci U S A 2008; 105: 1680-1685.
[40] Welsh J. Targets of vitamin D receptor signaling in the mammary gland. J Bone Miner Res 2007; 22 Suppl 2: V86-90.
[41] Lopes N, Paredes J, Costa JL, Ylstra B and Schmitt F. Vitamin D and the mammary gland: a review on its role in normal development and

breast cancer. Breast Cancer Res 2012; 14: 211.
[42] Zinser GM and Welsh J. Accelerated mammary gland development during pregnancy and delayed postlactational involution in vitamin D3 receptor null mice. Mol Endocrinol 2004; 18: 2208-2223.
[43] Zinser G, Packman K and Welsh J. Vitamin D(3) receptor ablation alters mammary gland morphogenesis. Development 2002; 129: 3067-3076.
[44] Cunha GR, Young P, Hom YK, Cooke PS, Taylor JA and Lubahn DB. Elucidation of a role for stromal steroid hormone receptors in mammary gland growth and development using tissue recombinants. J Mammary Gland Biol Neoplasia 1997; 2: 393-402.
[45] Humphreys RC, Lydon J, O'Malley BW and Rosen JM. Mammary gland development is mediated by both stromal and epithelial progesterone receptors. Mol Endocrinol 1997; 11: 801-811.
[46] Welsh J, Wietzke JA, Zinser GM, Byrne B, Smith K and Narvaez CJ. Vitamin D-3 receptor as a target for breast cancer prevention. J Nutr 2003; 133 Suppl: 2425s-2433s.
[47] Welsh J. Vitamin D and breast cancer: past and present. J Steroid Biochem Mol Biol 2018; 177: 15-20.
[48] ElShamy WM and Livingston DM. Identification of BRCA1-IRIS, a BRCA1 locus product. Nat Cell Biol 2004; 6: 954-967.
[49] Sinha A, Paul BT, Sullivan LM, Sims H, El Bastawisy A, Yousef HF, Zekri AN, Bahnassy AA and ElShamy WM. BRCA1-IRIS overexpression promotes and maintains the tumor initiating phenotype: implications for triple negative breast cancer early lesions. Oncotarget 2017; 8: 10114-10135.
[50] Blanchard Z, Paul BT, Craft B and ElShamy WM. BRCA1-IRIS inactivation overcomes paclitaxel resistance in triple negative breast cancers. Breast Cancer Res 2015; 17: 5.
[51] Bogan D, Meile L, El Bastawisy A, Yousef HF, Zekri AN, Bahnassy AA and ElShamy WM. The role of BRCA1-IRIS in the development and progression of triple negative breast cancers in Egypt: possible link to disease early lesion. BMC Cancer 2017; 17: 329.
[52] Shimizu Y, Luk H, Horio D, Miron P, Griswold M, Iglehart D, Hernandez B, Killeen J and ElShamy WM. BRCA1-IRIS overexpression promotes formation of aggressive breast cancers. PLoS One 2012; 7: e34102.
[53] Pettigrew CA, French JD, Saunus JM, Edwards SL, Sauer AV, Smart CE, Lundstrom T, Wiesner C, Spurdle AB, Rothnagel JA and Brown MA. Identification and functional analysis of novel BRCA1 transcripts, including mouse Brca1-Iris and human pseudo-BRCA1. Breast Cancer Res Treat 2010; 119: 239-247.
[54] Ryan D, Paul BT, Koziol J and ElShamy WM. The pro- and anti-tumor roles of mesenchymal stem cells toward BRCA1-IRIS-overexpressing TNBC cells. Breast Cancer Res 2019; 21: 53.
[55] Ryan D, Sinha A, Bogan D, Davies J, Koziol J and ElShamy WM. A niche that triggers aggressiveness within BRCA1-IRIS overexpressing triple negative tumors is supported by reciprocal interactions with the microenvironment. Oncotarget 2017; 8: 103182-103206.
[56] Paul BT, Blanchard Z, Ridgway M and ElShamy WM. BRCA1-IRIS inactivation sensitizes ovarian tumors to cisplatin. Oncogene 2015; 34: 3036-3052.
[57] Bahnassy A, Mohanad M, Ismail MF, Shaarawy S, El-Bastawisy A and Zekri AR. Molecular biomarkers for prediction of response to treatment and survival in triple negative breast cancer patients from Egypt. Exp Mol Pathol 2015; 99: 303-311.
[58] Bahhnassy A, Mohanad M, Shaarawy S, Ismail MF, El-Bastawisy A, Ashmawy AM and Zekri AR. Transforming growth factor-beta, insulin-like growth factor I/insulin-like growth factor I receptor and vascular endothelial growth factor-A: prognostic and predictive markers in triple-negative and non-triple-negative breast cancer. Mol Med Rep 2015; 12: 851-864.
[59] Oken MM, Creech RH, Tormey DC, Horton J, Davis TE, McFadden ET and Carbone PP. Toxicity and response criteria of the Eastern Cooperative Oncology Group. Am J Clin Oncol 1982; 5: 649-655.
[60] Thangamani S, Kim M, Son Y, Huang X, Kim H, Lee JH, Cho J, Ulrich B, Broxmeyer HE and Kim CH. Cutting edge: progesterone directly upregulates vitamin d receptor gene expression for efficient regulation of T cells by calcitriol. J Immunol 2015; 194: 883-886.
[61] Brisken C and Scabia V. 90 years of progesterone: progesterone receptor signaling in the normal breast and its implications for cancer. J Mol Endocrinol 2020; 65: T81-T94.
[62] Cai C, Geng A, Wang M, Yang L, Yu QC and Zeng YA. Amphiregulin mediates the hormonal regulation on Rspondin-1 expression in the mammary gland. Dev Biol 2020; 458: 43-51.
[63] Shimizu Y, Mullins N, Blanchard Z and Elshamy WM. BRCA1/p220 loss triggers BRCA1-IRIS overexpression via mRNA stabilization in breast cancer cells. Oncotarget 2012; 3: 299-313.
[64] Pascual R, Martín J, Salvador F, Reina O, Chanes V, Millanes-Romero A, Suñer C, Fernández-Miranda G, Bartomeu A, Huang YS, Gomis RR and Méndez R. The RNA binding protein CPEB2 regulates hormone sensing in mam-

mary gland development and luminal breast cancer. Sci Adv 2020; 6: eaax3868.
[65] Zhang Y, Si Y, Ma N and Mei J. The RNA-binding protein PCBP2 inhibits Ang II-induced hypertrophy of cardiomyocytes though promoting GPR56 mRNA degeneration. Biochem Biophys Res Commun 2015; 464: 679-684.
[66] Calvo V and Beato M. BRCA1 counteracts progesterone action by ubiquitination leading to progesterone receptor degradation and epigenetic silencing of target promoters. Cancer Res 2011; 71: 3422-3431.
[67] Rojas PA, May M, Sequeira GR, Elia A, Alvarez M, Martínez P, Gonzalez P, Hewitt S, He X, Perou CM, Molinolo A, Gibbons L, Abba MC, Gass H and Lanari C. Progesterone receptor isoform ratio: a breast cancer prognostic and predictive factor for antiprogestin responsiveness. J Natl Cancer Inst 2017; 109: djw317.
[68] Oakes SR, Rogers RL, Naylor MJ and Ormandy CJ. Prolactin regulation of mammary gland development. J Mammary Gland Biol Neoplasia 2008; 13: 13-28.
[69] Macias H and Hinck L. Mammary gland development. Wiley Interdiscip Rev Dev Biol 2012; 1: 533-557.
[70] Liu R, Zhou Z, Zhao D and Chen C. The induction of KLF5 transcription factor by progesterone contributes to progesterone-induced breast cancer cell proliferation and dedifferentiation. Mol Endocrinol 2011; 25: 1137-1144.
[71] Srivastava S, Matsuda M, Hou Z, Bailey JP, Kitazawa R, Herbst MP and Horseman ND. Receptor activator of NF-kappaB ligand induction via Jak2 and Stat5a in mammary epithelial cells. J Biol Chem 2003; 278: 46171-46178.
[72] Goffin V. Prolactin receptor targeting in breast and prostate cancers: new insights into an old challenge. Pharmacol Ther 2017; 179: 111-126.
[73] Sami E, Paul BT, Koziol JA and ElShamy WM. The immunosuppressive microenvironment in BRCA1-IRIS-overexpressing TNBC tumors is induced by bidirectional interaction with tumor-associated macrophages. Cancer Res 2020; 80: 1102-1117.
[74] Haricharan S and Li Y. STAT signaling in mammary gland differentiation, cell survival and tumorigenesis. Mol Cell Endocrinol 2014; 382: 560-569.
[75] Liao Z and Nevalainen MT. Targeting transcription factor Stat5a/b as a therapeutic strategy for prostate cancer. Am J Transl Res 2011; 3: 133-138.
[76] Nakuci E, Mahner S, Direnzo J and ElShamy WM. BRCA1-IRIS regulates cyclin D1 expression in breast cancer cells. Exp Cell Res 2006; 312: 3120-3131.
[77] Hao L and ElShamy WM. BRCA1-IRIS activates cyclin D1 expression in breast cancer cells by downregulating the JNK phosphatase DUSP3/VHR. Int J Cancer 2007; 121: 39-46.
[78] Prat A, Pineda E, Adamo B, Galvan P, Fernandez A, Gaba L, Diez M, Viladot M, Arance A and Muñoz M. Clinical implications of the intrinsic molecular subtypes of breast cancer. Breast 2015; 24 Suppl 2: S26-35.
[79] Khaled N and Bidet Y. New insights into the implication of epigenetic alterations in the EMT of triple negative breast cancer. Cancers (Basel) 2019; 11: 559.
[80] Collina F, Di Bonito M, Li Bergolis V, De Laurentiis M, Vitagliano C, Cerrone M, Nuzzo F, Cantile M and Botti G. Prognostic value of cancer stem cells markers in triple-negative breast cancer. Biomed Res Int 2015; 2015: 158682.
[81] Abell K, Bilancio A, Clarkson RW, Tiffen PG, Altaparmakov AI, Burdon TG, Asano T, Vanhaesebroeck B and Watson CJ. Stat3-induced apoptosis requires a molecular switch in PI(3)K subunit composition. Nat Cell Biol 2005; 7: 392-398.
[82] D'Amico S, Shi J, Martin BL, Crawford HC, Petrenko O and Reich NC. STAT3 is a master regulator of epithelial identity and KRAS-driven tumorigenesis. Genes Dev 2018; 32: 1175-1187.
[83] Nouhi Z, Chughtai N, Hartley S, Cocolakis E, Lebrun JJ and Ali S. Defining the role of prolactin as an invasion suppressor hormone in breast cancer cells. Cancer Res 2006; 66: 1824-1832.
[84] Borcherding DC, Hugo ER, Fox SR, Jacobson EM, Hunt BG, Merino EJ and Ben-Jonathan N. Suppression of breast cancer by small molecules that block the prolactin receptor. Cancers (Basel) 2021; 13: 2662.
[85] Linher-Melville K and Singh G. The transcriptional responsiveness of LKB1 to STAT-mediated signaling is differentially modulated by prolactin in human breast cancer cells. BMC Cancer 2014; 14: 415.
[86] Gonzalez-Suarez E, Jacob AP, Jones J, Miller R, Roudier-Meyer MP, Erwert R, Pinkas J, Branstetter D and Dougall WC. RANK ligand mediates progestin-induced mammary epithelial proliferation and carcinogenesis. Nature 2010; 468: 103-107.
[87] Sigl V and Penninger JM. RANKL/RANK-from bone physiology to breast cancer. Cytokine Growth Factor Rev 2014; 25: 205-214.
[88] Gonzalez-Suarez E, Branstetter D, Armstrong A, Dinh H, Blumberg H and Dougall WC. RANK overexpression in transgenic mice with mouse mammary tumor virus promoter-controlled RANK increases proliferation and impairs alveolar differentiation in the mammary epithelia and disrupts lumen formation in cultured

epithelial acini. Mol Cell Biol 2007; 27: 1442-1454.
[89] Welsh J, Wietzke JA, Zinser GM, Smyczek S, Romu S, Tribble E, Welsh JC, Byrne B and Narvaez CJ. Impact of the Vitamin D3 receptor on growth-regulatory pathways in mammary gland and breast cancer. J Steroid Biochem Mol Biol 2002; 83: 85-92.
[90] Thakkar A, Wang B, Picon-Ruiz M, Buchwald P and Ince TA. Vitamin D and androgen receptor-targeted therapy for triple-negative breast cancer. Breast Cancer Res Treat 2016; 157: 77-90.
[91] Chock K, Allison JM and Elshamy WM. BRCA1-IRIS overexpression abrogates UV-induced p38MAPK/p53 and promotes proliferation of damaged cells. Oncogene 2010; 29: 5274-5285.
[92] Silva VL, Ferreira D, Nobrega FL, Martins IM, Kluskens LD and Rodrigues LR. Selection of novel peptides homing the 4T1 CELL line: exploring alternative targets for triple negative breast cancer. PLoS One 2016; 11: e0161290.
[93] Hiraga T and Ninomiya T. Establishment and characterization of a C57BL/6 mouse model of bone metastasis of breast cancer. J Bone Miner Metab 2018; 37: 235-242.
[94] Bae SY, Jung SP, Jung ES, Park SM, Lee SK, Yu JH, Lee JE, Kim SW and Nam SJ. Clinical characteristics and prognosis of pregnancy-associated breast cancer: poor survival of luminal B subtype. Oncology 2018; 95: 163-169.
[95] Clarkson RW and Watson CJ. Microarray analysis of the involution switch. J Mammary Gland Biol Neoplasia 2003; 8: 309-319.
[96] Basree MM, Shinde N, Koivisto C, Cuitino M, Kladney R, Zhang J, Stephens J, Palettas M, Zhang A, Kim HK, Acero-Bedoya S, Trimboli A, Stover DG, Ludwig T, Ganju R, Weng D, Shields P, Freudenheim J, Leone GW, Sizemore GM, Majumder S and Ramaswamy B. Abrupt involution induces inflammation, estrogenic signaling, and hyperplasia linking lack of breastfeeding with increased risk of breast cancer. Breast Cancer Res 2019; 21: 80.
[97] Ericsson C and Nistér M. Protein extraction from solid tissue. Methods Mol Biol 2011; 675: 307-312.
[98] Li Z, Zhang X, Hou C, Zhou Y, Chen J, Cai H, Ye Y, Liu J and Huang N. Comprehensive identification and characterization of somatic copy number alterations in triple-negative breast cancer. Int J Oncol 2020; 56: 522-530.
[99] Ngan E, Stoletov K, Smith HW, Common J, Muller WJ, Lewis JD and Siegel PM. LPP is a Src substrate required for invadopodia formation and efficient breast cancer lung metastasis. Nat Commun 2017; 8: 15059.
[100] McAvoy S, Ganapathiraju SC, Ducharme-Smith AL, Pritchett JR, Kosari F, Perez DS, Zhu Y, James CD and Smith DI. Non-random inactivation of large common fragile site genes in different cancers. Cytogenet Genome Res 2007; 118: 260-269.
[101] Khaitan D, Sankpal UT, Weksler B, Meister EA, Romero IA, Couraud PO and Ningaraj NS. Role of KCNMA1 gene in breast cancer invasion and metastasis to brain. BMC Cancer 2009; 9: 258.
[102] Li CI, Beaber EF, Tang MT, Porter PL, Daling JR and Malone KE. Reproductive factors and risk of estrogen receptor positive, triple-negative, and HER2-neu overexpressing breast cancer among women 20-44 years of age. Breast Cancer Res Treat 2013; 137: 579-587.
[103] Tamimi RM, Colditz GA, Hazra A, Baer HJ, Hankinson SE, Rosner B, Marotti J, Connolly JL, Schnitt SJ and Collins LC. Traditional breast cancer risk factors in relation to molecular subtypes of breast cancer. Breast Cancer Res Treat 2012; 131: 159-167.
[104] Newcomb PA, Storer BE, Longnecker MP, Mittendorf R, Greenberg ER, Clapp RW, Burke KP, Willett WC and MacMahon B. Lactation and a reduced risk of premenopausal breast cancer. N Engl J Med 1994; 330: 81-87.
[105] Gaudet MM, Press MF, Haile RW, Lynch CF, Glaser SL, Schildkraut J, Gammon MD, Douglas Thompson W and Bernstein JL. Risk factors by molecular subtypes of breast cancer across a population-based study of women 56 years or younger. Breast Cancer Res Treat 2011; 130: 587-597.
[106] Layde PM, Webster LA, Baughman AL, Wingo PA, Rubin GL and Ory HW. The independent associations of parity, age at first full term pregnancy, and duration of breastfeeding with the risk of breast cancer. Cancer and Steroid Hormone Study Group. J Clin Epidemiol 1989; 42: 963-973.
[107] Watson CJ. Involution: apoptosis and tissue remodelling that convert the mammary gland from milk factory to a quiescent organ. Breast Cancer Res 2006; 8: 203.
[108] Stein T, Morris JS, Davies CR, Weber-Hall SJ, Duffy MA, Heath VJ, Bell AK, Ferrier RK, Sandilands GP and Gusterson BA. Involution of the mouse mammary gland is associated with an immune cascade and an acute-phase response, involving LBP, CD14 and STAT3. Breast Cancer Res 2004; 6: R75-91.
[109] Dado-Senn B, Skibiel AL, Fabris TF, Zhang Y, Dahl GE, Peñagaricano F and Laporta J. RNA-Seq reveals novel genes and pathways involved in bovine mammary involution during the dry period and under environmental heat stress. Sci Rep 2018; 8: 11096.

[110] Yoo KY, Tajima K, Kuroishi T, Hirose K, Yoshida M, Miura S and Murai H. Independent protective effect of lactation against breast cancer: a case-control study in Japan. Am J Epidemiol 1992; 135: 726-733.
[111] Russo J, Tay LK and Russo IH. Differentiation of the mammary gland and susceptibility to carcinogenesis. Breast Cancer Res Treat 1982; 2: 5-73.
[112] Romieu I, Hernandez-Avila M, Lazcano E, Lopez L and Romero-Jaime R. Breast cancer and lactation history in Mexican women. Am J Epidemiol 1996; 143: 543-552.
[113] McTiernan A and Thomas DB. Evidence for a protective effect of lactation on risk of breast cancer in young women. Results from a case-control study. Am J Epidemiol 1986; 124: 353-358.
[114] Byers T, Graham S, Rzepka T and Marshall J. Lactation and breast cancer. Evidence for a negative association in premenopausal women. Am J Epidemiol 1985; 121: 664-674.
[115] Bambhroliya A, Van Wyhe RD, Kumar S, Debeb BG, Reddy JP, Van Laere S, El-Zein R, Rao A and Woodward WA. Gene set analysis of post-lactational mammary gland involution gene signatures in inflammatory and triple-negative breast cancer. PLoS One 2018; 13: e0192689.
[116] Mamouch F, Berrada N, Aoullay Z, El Khanoussi B and Errihani H. Inflammatory breast cancer: a literature review. World J Oncol 2018; 9: 129-135.
[117] Feng W, Liu S, Zhu R, Li B, Zhu Z, Yang J and Song C. SOX10 induced Nestin expression regulates cancer stem cell properties of TNBC cells. Biochem Biophys Res Commun 2017; 485: 522-528.
[118] O'Conor CJ, Chen T, González I, Cao D and Peng Y. Cancer stem cells in triple-negative breast cancer: a potential target and prognostic marker. Biomark Med 2018; 12: 813-820.
[119] Song Y, Zhao B, Xu Y, Ren X, Lin Y, Zhou L and Sun Q. Prognostic significance of branched-chain amino acid transferase 1 and CD133 in triple-negative breast cancer. BMC Cancer 2020; 20: 584.
[120] Liu P, Tang H, Song C, Wang J, Chen B, Huang X, Pei X and Liu L. SOX2 promotes cell proliferation and metastasis in triple negative breast cancer. Front Pharmacol 2018; 9: 942.
[121] Yao GD, Niu YY, Chen KX, Meng HX, Yao GD, Song HT, Tian ZN, Geng JS and Feng MY. SOX2 gene expression and its role in triple negative breast cancer tissues. J Biol Regul Homeost Agents 2018; 32: 1399-1406.
[122] Fernandez-Valdivia R, Mukherjee A, Creighton CJ, Buser AC, DeMayo FJ, Edwards DP and Lydon JP. Transcriptional response of the murine mammary gland to acute progesterone exposure. Endocrinology 2008; 149: 6236-6250.
[123] Bachelot A and Binart N. Corpus luteum development: lessons from genetic models in mice. Curr Top Dev Biol 2005; 68: 49-84.
[124] Katiyar P, Ma Y, Riegel A, Fan S and Rosen EM. Mechanism of BRCA1-mediated inhibition of progesterone receptor transcriptional activity. Mol Endocrinol 2009; 23: 1135-1146.
[125] Barash I. Stat5 in breast cancer: potential oncogenic activity coincides with positive prognosis for the disease. Carcinogenesis 2012; 33: 2320-2325.
[126] Brandebourg TD, Bown JL and Ben-Jonathan N. Prolactin upregulates its receptors and inhibits lipolysis and leptin release in male rat adipose tissue. Biochem Biophys Res Commun 2007; 357: 408-413.
[127] Clarkson RW, Boland MP, Kritikou EA, Lee JM, Freeman TC, Tiffen PG and Watson CJ. The genes induced by signal transducer and activators of transcription (STAT)3 and STAT5 in mammary epithelial cells define the roles of these STATs in mammary development. Mol Endocrinol 2006; 20: 675-685.
[128] Lund LR, Bjørn SF, Sternlicht MD, Nielsen BS, Solberg H, Usher PA, Osterby R, Christensen IJ, Stephens RW, Bugge TH, Danø K and Werb Z. Lactational competence and involution of the mouse mammary gland require plasminogen. Development 2000; 127: 4481-4492.
[129] Li M, Liu X, Robinson G, Bar-Peled U, Wagner KU, Young WS, Hennighausen L and Furth PA. Mammary-derived signals activate programmed cell death during the first stage of mammary gland involution. Proc Natl Acad Sci U S A 1997; 94: 3425-3430.
[130] Creamer BA, Sakamoto K, Schmidt JW, Triplett AA, Moriggl R and Wagner KU. Stat5 promotes survival of mammary epithelial cells through transcriptional activation of a distinct promoter in Akt1. Mol Cell Biol 2010; 30: 2957-2970.
[131] Walker SR, Xiang M and Frank DA. Distinct roles of STAT3 and STAT5 in the pathogenesis and targeted therapy of breast cancer. Mol Cell Endocrinol 2014; 382: 616-621.
[132] Monks J and Henson PM. Differentiation of the mammary epithelial cell during involution: implications for breast cancer. J Mammary Gland Biol Neoplasia 2009; 14: 159-170.
[133] van der Rhee H, Coebergh JW and de Vries E. Sunlight, vitamin D and the prevention of cancer: a systematic review of epidemiological studies. Eur J Cancer Prev 2009; 18: 458-475.
[134] Janowsky EC, Lester GE, Weinberg CR, Millikan RC, Schildkraut JM, Garrett PA and Hulka BS. Association between low levels of 1,25-dihydroxyvitamin D and breast cancer risk. Public Health Nutr 1999; 2: 283-291.

[135] Rainville C, Khan Y and Tisman G. Triple negative breast cancer patients presenting with low serum vitamin D levels: a case series. Cases J 2009; 2: 8390.
[136] Peppone LJ, Rickles AS, Janelsins MC, Insalaco MR and Skinner KA. The association between breast cancer prognostic indicators and serum 25-OH vitamin D levels. Ann Surg Oncol 2012; 19: 2590-2599.
[137] Harvell DM, Kim J, O'Brien J, Tan AC, Borges VF, Schedin P, Jacobsen BM and Horwitz KB. Genomic signatures of pregnancy-associated breast cancer epithelia and stroma and their regulation by estrogens and progesterone. Horm Cancer 2013; 4: 140-153.
[138] Yuan JM, Yu MC, Ross RK, Gao YT and Henderson BE. Risk factors for breast cancer in Chinese women in Shanghai. Cancer Res 1988; 48: 1949-1953.
[139] Tao SC, Yu MC, Ross RK and Xiu KW. Risk factors for breast cancer in Chinese women of Beijing. Int J Cancer 1988; 42: 495-498.
[140] Rosero-Bixby L, Oberle MW and Lee NC. Reproductive history and breast cancer in a population of high fertility, Costa Rica, 1984-85. Int J Cancer 1987; 40: 747-754.
[141] Brinton LA, Potischman NA, Swanson CA, Schoenberg JB, Coates RJ, Gammon MD, Malone KE, Stanford JL and Daling JR. Breastfeeding and breast cancer risk. Cancer Causes Control 1995; 6: 199-208.
[142] Jeong SH, An YS, Choi JY, Park B, Kang D, Lee MH, Han W, Noh DY, Yoo KY and Park SK. Risk reduction of breast cancer by childbirth, breastfeeding, and their interaction in Korean women: heterogeneous effects across menopausal status, hormone receptor status, and pathological subtypes. J Prev Med Public Health 2017; 50: 401-410.
[143] Enger SM, Ross RK, Henderson B and Bernstein L. Breastfeeding history, pregnancy experience and risk of breast cancer. Br J Cancer 1997; 76: 118-123.
[144] Ning Y, Hoang B, Schuller AG, Cominski TP, Hsu MS, Wood TL and Pintar JE. Delayed mammary gland involution in mice with mutation of the insulin-like growth factor binding protein 5 gene. Endocrinology 2007; 148: 2138-2147.
[145] Lochrie JD, Phillips K, Tonner E, Flint DJ, Allan GJ, Price NC and Beattie J. Insulin-like growth factor binding protein (IGFBP)-5 is upregulated during both differentiation and apoptosis in primary cultures of mouse mammary epithelial cells. J Cell Physiol 2006; 207: 471-479.
[146] Shema L, Ore L, Ben-Shachar M, Haj M and Linn S. The association between breastfeeding and breast cancer occurrence among Israeli Jewish women: a case control study. J Cancer Res Clin Oncol 2007; 133: 539-546.
[147] Chock KL, Allison JM, Shimizu Y and ElShamy WM. BRCA1-IRIS overexpression promotes cisplatin resistance in ovarian cancer cells. Cancer Res 2010; 70: 8782-8791.
[148] Segawa K and Nagata S. An apoptotic 'eat me' signal: phosphatidylserine exposure. Trends Cell Biol 2015; 25: 639-650.

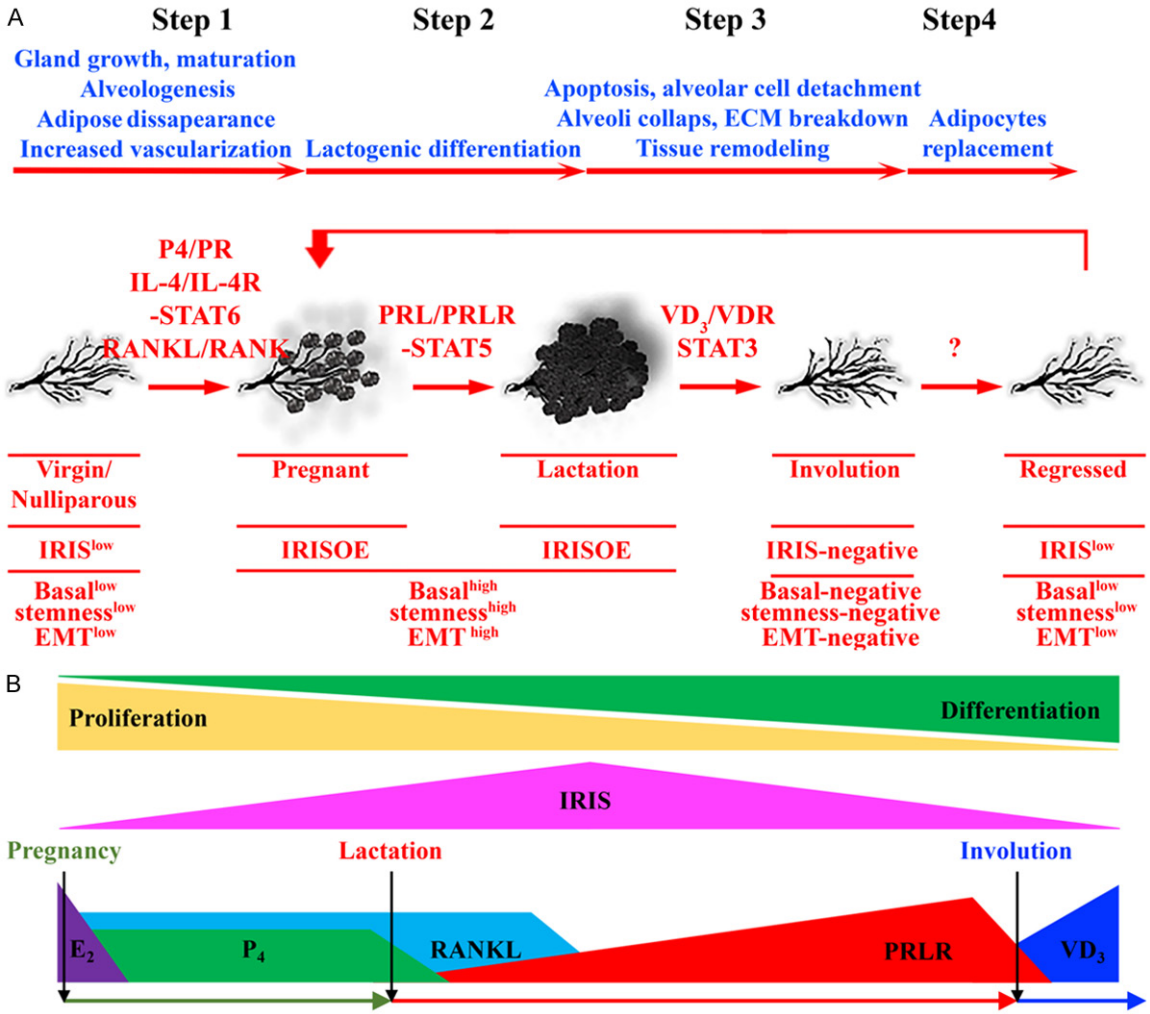

Figure S1. Overview of mammary gland development. A. Stages and corresponding changes in the adult female mammary gland during nulliparous/virgin, pregnancy, lactation, involution, and regression stages correlated with changes in IRIS, and basal, stemness, and EMT biomarkers expression. B. Representative presentation of the mammary gland stages super exposed on the status, IRIS expression and level of the different hormones, and growth factors in the mammary gland.

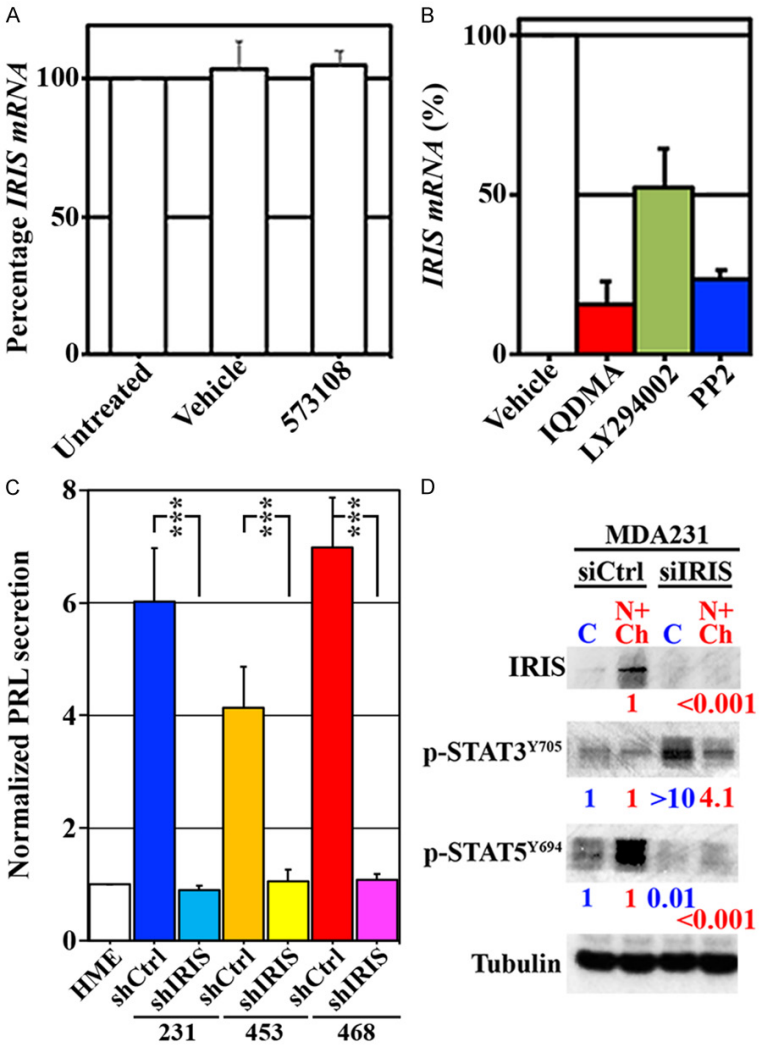

Figure S2. Effect of several signaling on IRIS mRNA expression and the effect of IRISOE on the STAT activation. (A) Normalized IRIS mRNA expression in PRLR^{+ve}-HME cells treated with vehicle or 573108 (inset) in the absence of PRL treatment for 24 h. (B) Normalized IRIS mRNA expression in PRLR^{+ve}-HME cells treated with 1 μM of PRL with vehicle, IQMDA, LY294002, or PP2 for 24 h. (C, D) Expression of IRIS, Y705-phosphorylated STAT3, and Y694-phosphorylated STAT5 in cytoplasmic (C) or nuclear + chromatin (N+Ch) extracts from MDA-MB231 cell lines transfected with siLuc or siIRIS (D). In all parts n=3.

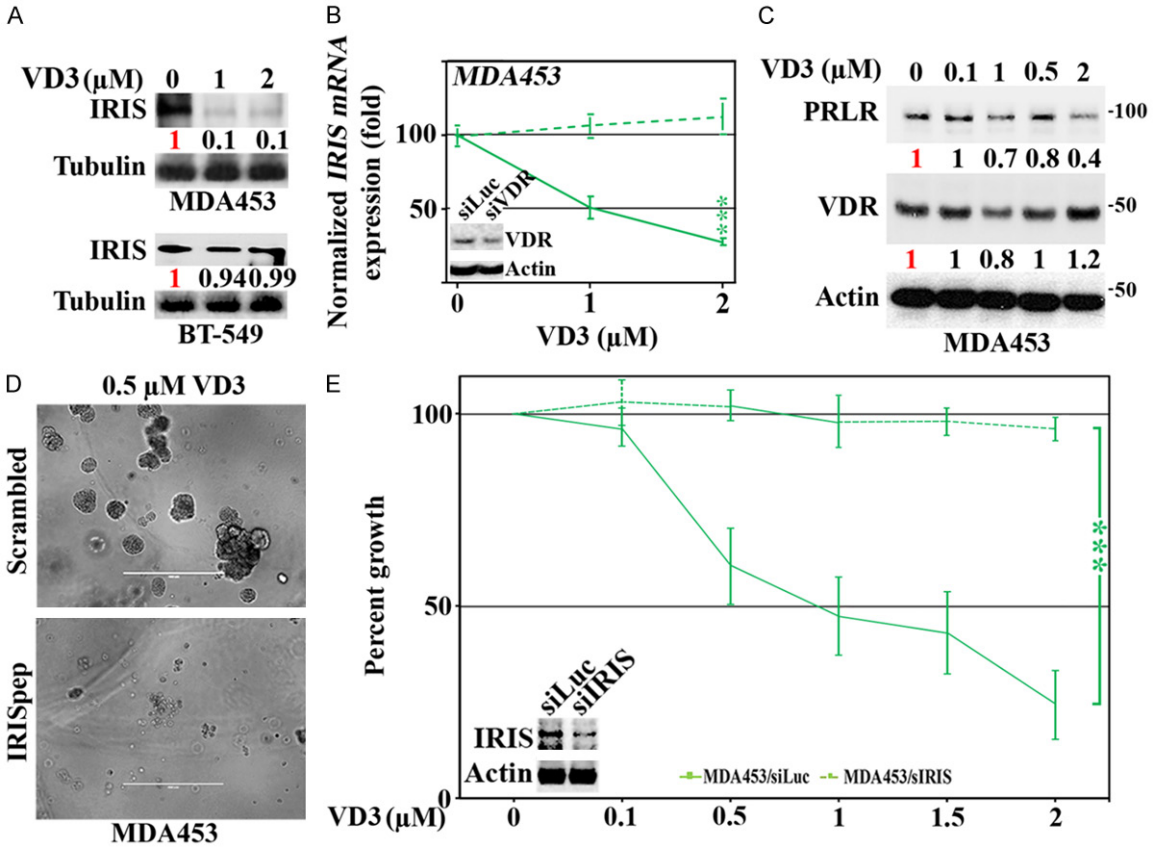

Figure S3. Negative feedback loop between IRISOE and VD_3/VDR activity in IRISOE-TNBC cells. Expression of IRIS in MDA453, BT-549 cells 24 h after treatment with the indicated VD_3 concentrations. Data presented are representative of 3 separate times. B. Normalized IRIS mRNA expression in MDA453 cells pre-silenced from control or VDR for 48 h followed by treatment with the indicated concentration of VD_3 for an additional 24 h. Data presented are from triplicates done three separate times. Inset shows the expression of VDR in these cells at 48 h after transfection. C. PRLR and VDR expression in MDA453 cell line treated with increasing concentrations of VD_3 for 24 h. D. MSFs assay in Matrigel using MDA453 cells treated with scrambled or IRISpep plus 0.5 μM of VD_3 for 24 h. E. Percentage of growth of MDA453 cells transfected with siLuc or siIRIS for 48 h (inset) then in SF-media with increasing concentrations of VD_3. In all parts n=3.

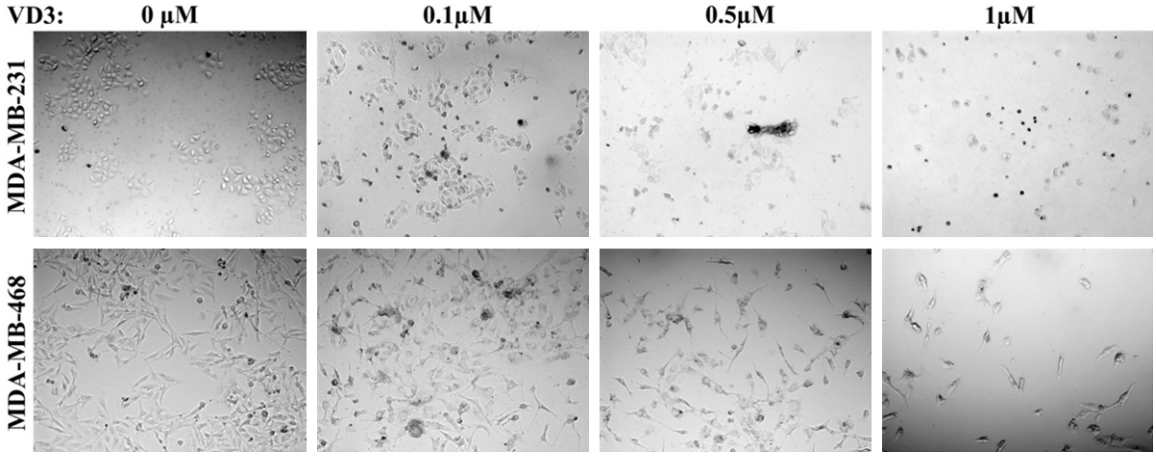

Figure S4. VD_3 effect on TNBC survival. Representative images of MDA231 (upper panels), MDA468 (lower panels) following treatment with the indicated concentrations of VD_3 for 96 h. In all parts n=3.

A

IRIS5 + Lactating extracts				
	-Dox		+Dox	
	Scram	IRISpep	Scram	IRISpep
Sub-G1	3.5±0.6	3.3±1.1	4.1±1.4	10.9±3.1
G0/G1	60.7±0.5	60.7±1.1	38.5±4.2	57.1±1.4
S	12.1±1.4	13±1.6	36.7±2.5	7.9±1.1
G2/M	20.9±2.5	20.4±3.2	16.7±1.1	21.7±3.1
>4N	3.1±1.6	2.6±1.9	3.8±0.7	2.9±1.6
p-values		vs. -Dox Scram	vs. -Dox Scram	vs. +Dox Scram
Sub-G1		0.8271	0.5431	0.0257
G0/G1		0.9629	0.0008	0.0019
S		0.5205	0.0001	<0.0001
G2/M		0.84412	<0.0565	0.0054
>4N		0.7927	0.4615	0.4408

B

IRIS5 + Involuting extracts				
	-Dox		+Dox	
	Scram	IRISpep	Scram	IRISpep
Sub-G1	21.9±1.6	20.9±0.8	4.6±0.2	22.5±2.1
G0/G1	32.9±1.1	32.4±0.9	38.3±3.1	33.2±2.3
S	11.2±1.1	10.1±0.3	16.9±1.5	11.9±1.9
G2/M	31.3±1.1	33.9±0.7	16.4±1.0	30.5±0.5
>4N	2.6±0.4	2.5±1.8	23.7±1.8	1.8±0.4
p-values		vs. -Dox Scram	vs. -Dox Scram	vs. +Dox Scram
Sub-G1		0.3895	<0.0001	0.0001
G0/G1		0.2141	0.0447	0.0797
S		0.2018	0.0061	0.0244
G2/M		0.0242	<0.0001	<0.0001
>4N		0.9081	<0.0001	<0.0001

Figure S5. Involution microenvironment promotes cell death in $IRIS^{-ve}$ cells and aneuploidy in IRISOE cells. (A and B) Percentage of cells showing sub-G1-, G0/G1-, S-, G2/M-, and >4N-cell cycle profile in IRIS5 cell line when IRIS expression is not induced (-Dox, i.e., $IRIS^{-ve}$) or induced (+Dox, i.e., IRISOE) when treated with 500 µg of L-d10 (**Figure 6F**) or l-d2 (**Figure 6G**) C57BL/6 mice mammary glands (n=3ea, combined) in the presence of scrambled or **IRIS**-pep. Assays were repeated 3 separate times.

A

Ch	1	2	3	4	5	6	7	8	9	10	11	12	13	14	15	16	17	18	19	20	21	22	X
Gain	p34	q12	q27 -28	-	-	-	-	p11, q21	q21	q22	p14	-	-	q21	-	q21	p11	p11	-	p12	-	-	-
Loss	q31	q13	q26	q13	q5, q14, q21	q12	q31	-	p21, q31	q21	q14	-	q31	q22	-	q23	-	-	-	-	-	-	p22.33 -q28

B

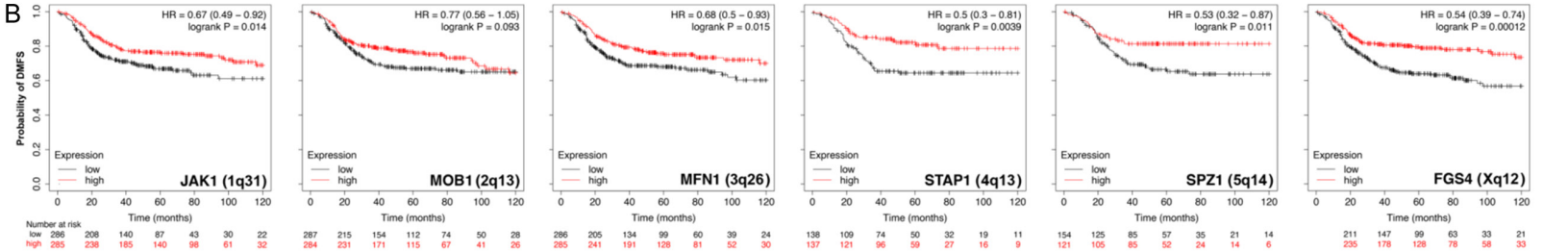

C

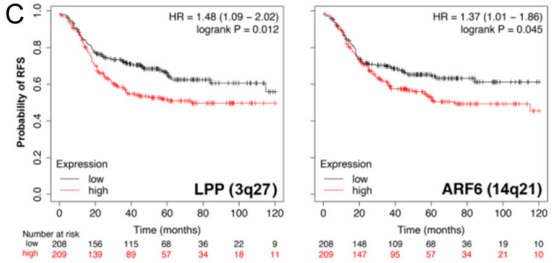

Figure S6. Aneuploidy induced by IRISOE in HME cells is associated with DMFS and RFS in breast cancer patients. (A) Positions of chromosomal gains and losses in 1°-orthotopic IRISOE mammary tumors developed in athymic mice using inducible-IRIS expressing HME cells as detected with CGH. (B) Kaplan Meier association of DMFS with genes identified as lost in IRISOE tumors in (A) in a breast tumor cohort. (C) Kaplan Meier association of RFS with genes identified as gained in IRISOE tumors in (A) in a breast tumor cohort.

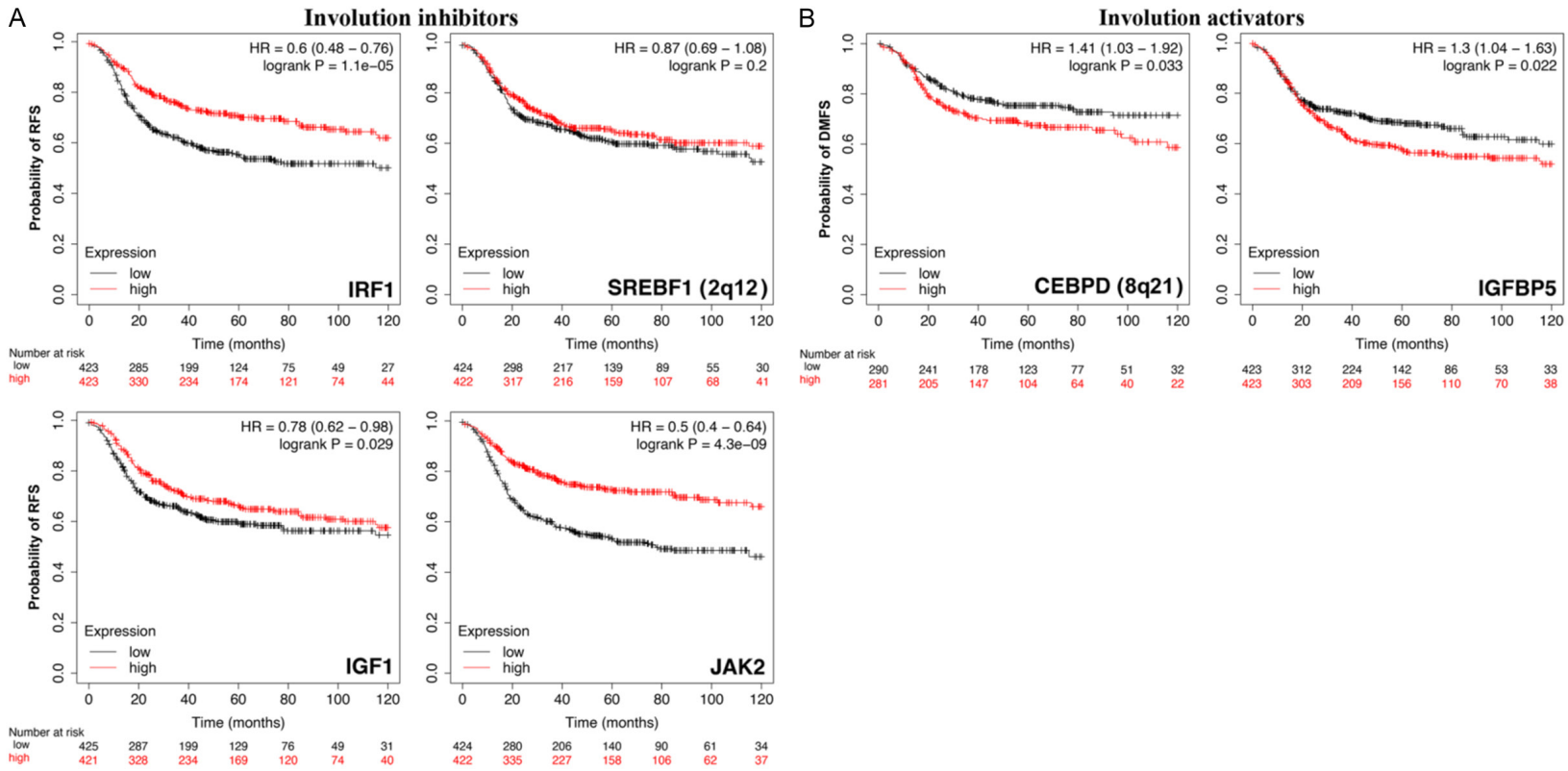

Figure S7. Involution associated inhibitors and activators association with RFS and DMFS in breast cancer patients. (A and B) Kaplan Meier analysis of breast tumors samples for the association of genes involved in inhibiting involution with RFS (A) or activating involution with DMFS (B).

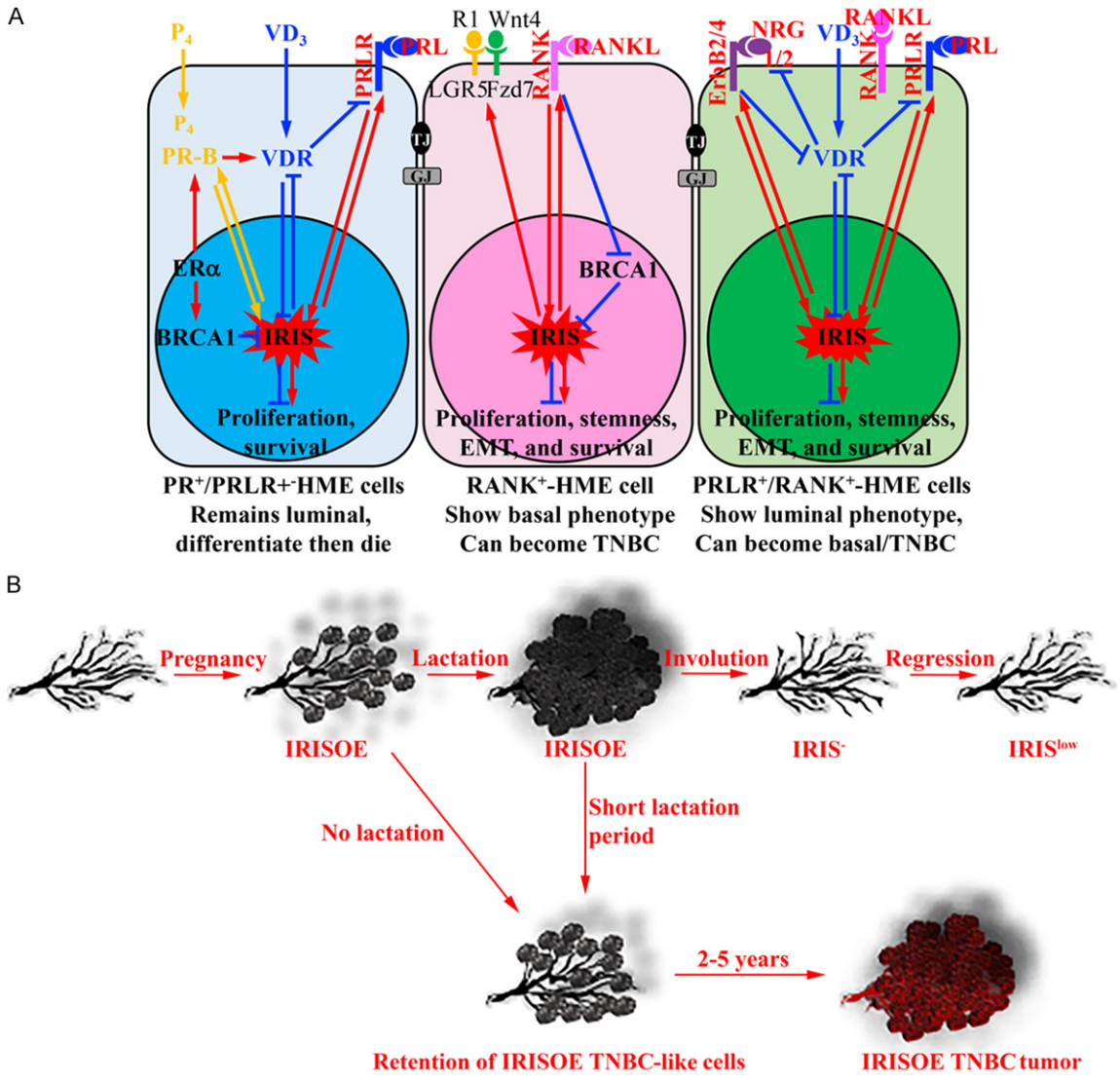

Figure S8. IRISOE induces PABC. A. Representative presentation of the 3 types mammary epithelial cells in human (and mouse) showing the effect of the hormones, cytokines, and growth factors on IRIS expression and the fate of these IRISOE-different mammary cell types. B. Representative presentation of the overall hypothesis emphasizing the positive role of longer-period of breastfeeding in preventing persistence of IRISOE cells in the mammary gland that can develop into TNBC tumors at later stages. This breaks when no or short-term lactation occurs leading to breast cancer.